LEVEL

PULSE POWER SWITCH DEVELOPMENT

R. Harvey, H. Gallagher, and S. Hansen

Hughes Research Laboratories
3011 Malibu Canyon Road
Malibu, CA 90265

October 1980

Approved for public release; distribution unlimited.

The views and conclusions contained in this document are those of the authors and should not be interpreted as representing the official policies, either expressed or implied, of the Defense Advanced Research Projects Agency or the U. S. Government.

80 10 10 020

REPORT DOCUMENTATION PAGE

READ INSTRUCTIONS
BEFORE COMPLETING FORM

1. REPORT NUMBER	2. GOVT ACCESSION NO.	3. RECIPIENT'S CATALOG NUMBER
	AD-A090 511	

4. TITLE (and Subtitle)	5. TYPE OF REPORT & PERIOD COVERED
PULSE POWER SWITCH DEVELOPMENT.	Final rept, 19 Sep — 18 Jan 1980
	6. PERFORMING ORG. REPORT NUMBER 19 Sep 79 - 18 Jan 80,

7. AUTHOR(s)	8. CONTRACT OR GRANT NUMBER(s)
R. Harvey, H. Gallagher, S. Hansen	N60921-79-C-0276 ARPA Order-3718

9. PERFORMING ORGANIZATION NAME AND ADDRESS	10. PROGRAM ELEMENT, PROJECT, TASK AREA & WORK UNIT NUMBERS
Hughes Research Laboratories 3011 Malibu Canyon Road Malibu, CA 90265	ARPA Order No. 3718 61101E;0;0;OR40AA

11. CONTROLLING OFFICE NAME AND ADDRESS	12. REPORT DATE
Defense Advanced Research Projects Agency 1400 Wilson Blvd., Arlington, VA 22209 Attn: Program Management/MIS	October 1980
	13. NUMBER OF PAGES 66

14. MONITORING AGENCY NAME & ADDRESS(if different from Controlling Office)	15. SECURITY CLASS. (of this report)
Naval Surface Weapons Center Silver Springs, MD 20910 Attn: Code R401	UNCLASSIFIED
	15a. DECLASSIFICATION DOWNGRADING SCHEDULE

16. DISTRIBUTION STATEMENT (of this Report)

Approved for public release; distribution unlimited.

17. DISTRIBUTION STATEMENT (of the abstract entered in Block 20, if different from Report)

18. SUPPLEMENTARY NOTES

19. KEY WORDS (Continue on reverse side if necessary and identify by block number)

Switch, High repetition rate, High power, Crossatron switch, Vacuum spark gaps, pressurized spark gaps

20. ABSTRACT (Continue on reverse side if necessary and identify by block number)

The objective of this study program has been to define an optimum technical approach to the longer range goal of achieving practical high repetition rate high power "spark gap" switches. Requirements and possible means of extending the state of the art of crossed field closing switches, vacuum spark gaps, and pressurized spark gaps are presented with emphasis on reliable, efficient and compact devices operable in burst mode at 250-300 kV, 40-60 kA, >1 kHz with ~50 nsec

DD FORM 1473 EDITION OF 1 NOV 65 IS OBSOLETE
1 JAN 73

172600 APPROXIMATELY

APPROXIMATELY

pulses rising in 3 ns. Models of these devices are discussed which are based upon published and generated design data and on underlying physical principles. Based upon its relative advantages, limitations and tradeoffs we conclude that the Hughes Crossatron switch is the nearest term approach to reach the switch goal levels. Theoretical, experimental, and computer simulation models of the plasma show a collective ion acceleration mechanism to be active which is predicted to result in current rise times approaching 10 nsec. A preliminary design concept is presented. For faster risetimes we have shown a vacuum surface flashover switch to be an interesting candidate. This device is limited by trigger instabilities and will require further basic development. The problem areas relevant to high pressure spark gaps are reviewed. Here we suggest that small, high pressure, self contained gaps meeting complex design criteria may be required for high repetition rates and high efficiency.

TABLE OF CONTENTS

LIST OF ILLUSTRATIONS

SECTION I

INTRODUCTION AND SUMMARY

The long range objective of this program has been to develop
practical high repetition rate, high power "spark gap" switches suitable
for particle beam weapons systems and related applications such as con-
trolled thermonuclear fusion. This preliminary study phase has been
devoted to developing criteria and means for extending the state of the
art of crossed field closing switches, vacuum spark gaps and pressurized
spark gaps to meet the goal levels[1] shown in Table 1. Based upon its
relative advantages, limitations and tradeoffs, we have concluded that
the Hughes Crossatron[2] switch appears to be the nearest term approach
to reach prototype switch goal levels of 250-300 kV, 40-60 kA, and
>1 kHz. Switch operation at rise times less than ∿10 ns may require an
alternative approach. To this end we have demonstrated a field emitter
triggered vacuum surface flashover switch, with an inherent capability
of achieving rise times of a few nanoseconds. It is presently limited
by trigger instabilities and requires more basic development. The prob-
lem areas critical to the further development of pressurized spark
gaps have been organized in a form which implies that small, high
pressure, self contained, flowing gas units meeting complex design
criteria will be required in order to achieve high repetition rates at
practical efficiencies.

Table 1. Switch Goal Levels[1]

Parameter	Goal
Peak current	40-60 kA
Peak voltage	250-300 kV
Average current	20 A
Repetition rate	> 1 kHz
Anode fall time	3 nsec
Maximum inductance or characteristic impedance	18 nH, or 6.25Ω
Maximum jitter	1 nsec
Pulse width	50 nsec

7

The Hughes Crossatron switch is a hybrid crossed field device suitable for high frequency operation. Figure 1 shows a projected HV design which utilizes the following features. The switch is approximately matched to the transmission lines (or Blumlein) at either end by an insulating transition which is made slightly conductive to insure a uniform potential distribution. The central anode electrode is normally isolated from the return path at the source section by low pressure He gas. Just prior to the desired trigger time a weak crossed field discharge current in the source section is increased until the source current reaches the desired anode current and the plasma from the source expands to reach the negatively biased control grid. The control grid is then pulsed positive and the plasma is abruptly released to cross the gap. Following the main switching pulse the source current is turned off and the switch resets.

Crossatron switches using such multiple electrode structures have been tested at low power and high repetion rates (10 kHz). Theoretical analyses show that the plasma transport across the gap is enhanced by collective acceleration with ions reaching energies nearly an order of magnitude higher than the electron thermal temperature. This mechanism results in a short current rise time and relies on an initial high current density in the source plasma. A review of the data for the Crossation test models shows agreement with the theory with measured rise times as short as 10-15 ns at 100A. We anticipate that a high power model will require a segmented source section as shown (Figure 1) in order to avoid unwanted plasma instabilities. The operating pressure would be on the order of 25 mTorr. This minimizes charge exchange effects and also should allow spacings in the HV section of at least 4 cm without danger of Paschen breakdown. The details of this approach and a higher pressure backup approach are presented in Section II.

Vacuum spark gaps are fast recovery devices which have typically relied upon the transport of vaporized material, gasses, or plasma across a gap in order to strike an arc and to neutralize the electronic space charge.[2,3] These transport mechanisms are relatively slow and involve erosion of the electrodes in some form. A dielectric surface
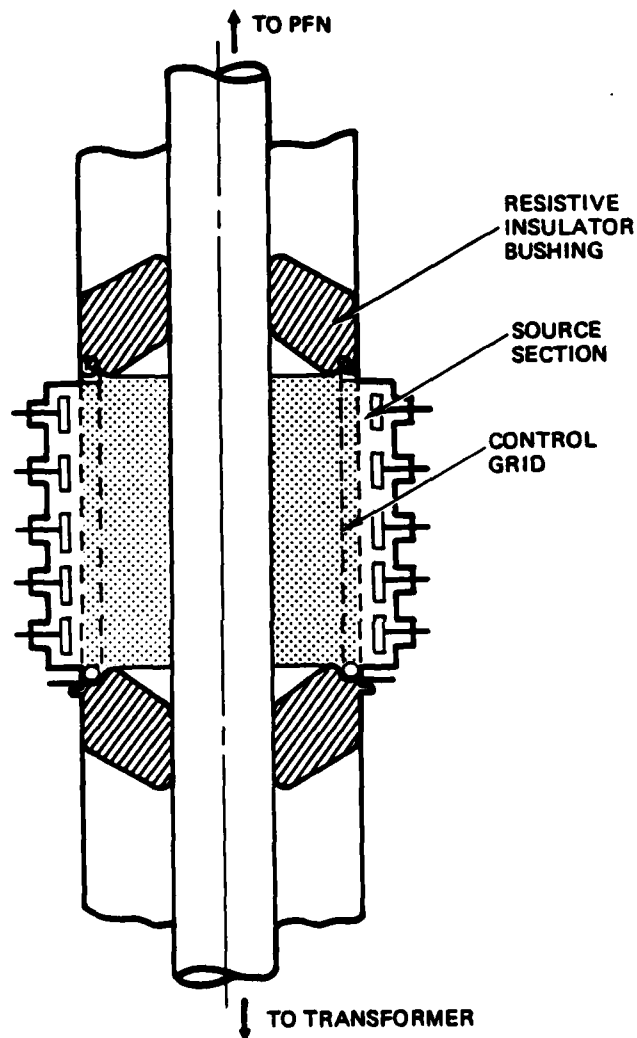
9497-24

Figure 1. Preliminary crossatron switch design
for 250-300 kV, 40-60 kA, >1 kA opera-
tion with current rise times ∿10 ns.

9

in vacuum represents a source of secondary electrons and neutralizing stationary ions.[4,5,6] If a suitable means were found to stabilize the surface charge and then initiate an electron avalanche (which did not erode the surface), then one would have the basis for an intrinsically high speed switch. We have been able to demonstrate some of the rudiments of such high speed switching by utilizing a low power field emitting triple point junction (vacuum-insulator-metal) as a triggered source of electrons. These electrons cascade to the cathode and then avalanche down an insulator to the anode, resulting in a flashover of the insulator. The most important problem with this switch is that the insulator state does not appear to be the same from pulse to pulse and the jitter time is excessive. Potentially, however, it is expected to have a recovery time characteristic of other vacuum devices ($\lesssim 100$ μs) in addition to a switching speed on the order of nanoseconds. This vacuum surface switch work is discussed in Section III.

Pressurized spark gaps are capable of operating at current and voltage levels well into the region of interest.[7] Rise times and jitter are also satisfactory. However high repetition rate operation (> 1 kHz) poses a difficult problem. It might be possible to find a combination of gasses whose recovery and recombination rates are high enough but this is likely to require high pressure operation sensitive to serious mechanical alignment and electrode wear problems. Alternatively (or in combination with the above) turbulent aerodynamic sweepout and cooling of the conductive arc remnants will be required. A series of problems are established under these conditions which are likely to necessitate a complex set of design criteria. These include drag losses, laminar and turbulent cavitation, shock waves, acoustical waves, random upstream flow, and local flow stagnation. Small sizes and closed gas flow loop are necessary to reduce both drag losses and large enthalpy losses in the gas. These and other criteria are discussed in Section IV.

The propagation of plasma across a vacuum in the presence of a high electric field is of fundamental importance to Crossatron and similar switches. Theoretical and computer simulation models of the

plasma motion are discussed in Section V. The electron flux to the anode is limited by space charge effects and the thermal motion of the electrons generates a potential minima at the edge of the plasma. The depth of this potential minimum regulates the electron current to the anode. Ions at the plasma surface are accelerated towards the anode and would pick up an amount of energy equivalent to the potential drop. However, as the ions move towards the minimum, the minimum also moves. Consequently, the ions are able to reach velocities well in excess of the minimum potential by this collective mechanism. Only a relatively small amount of ionic space charge is required to neutralize the higher speed electron flow. The overall current rise time is shown to be a function of the voltage, gap spacing, electron temperature and the initial source current. Based on this information, a Crossatron type of device designed to operate at a low fill pressure (to achieve a maximum electron temperature and/or a hot tail of 10 to 100 eV) with a gap spacing $\lesssim 4$ cm and a pulsed source current density of 100 A/cm^2 should be capable of a 10-20 ns current rise time at 250-300 kV.
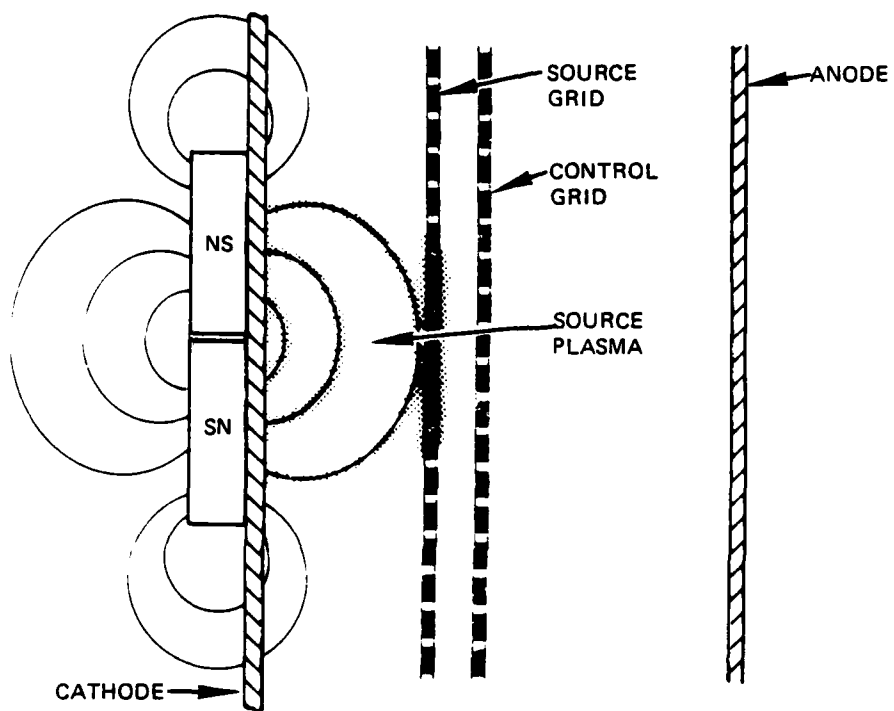
SECTION II

CROSSATRON

Introduction

The Crossatron is a hybrid switching device suitable for high frequency operation. It uses a crossed-field discharge generated plasma as a source of charge carriers and is grid controlled. The coaxial electrode structures shown in Figure 2 include: an anode, a cathode, a source grid and a control grid. A dc magnetic field (localized to the gap between the source grid and the cathode) is used to sustain the source plasma when that grid is energized. This plasma runs at a voltage drop of $\sim$250 V and is an adjustable source of charges analogous to a thermionic emitter with a negligible thermal inertia. The anode current is controlled by the control grid potential. This provides for exceptionally short response times and high repetition rate operation.

Test Model

A low power test model (Figure 3) had been operated as a closing switch to 10 kHz at 15 kV; and in addition shows a current rise time of 28 nsec at anode currents and voltages of up to 1750 A and 30 kV. Even shorter rise times (10-15 nsec) have been observed when the anode and source currents are comparable (Figure 4). Originally, the test model was operated without a control grid. In this case repetitive switching rates exceed 16 kHz using the source plasma to switch the device. Since the source plasma is inherently slow to develop ($\sim$0.1 µs), this triode mode of operation is suitable for applications with relatively slow rise times, and where the jitter time is not important.

For higher speed operation a tetrode mode is used. A control grid is included to contain the source plasma until it reaches a high density. This is done by biasing the control grid about 300 V negative, effectively cutting off any significant anode conduction. The control grid is then abruptly pulsed positive, resulting in a rapid current rise time.

13

Figure 2. Crossatron switch electrode structure and source section schematic drawing.

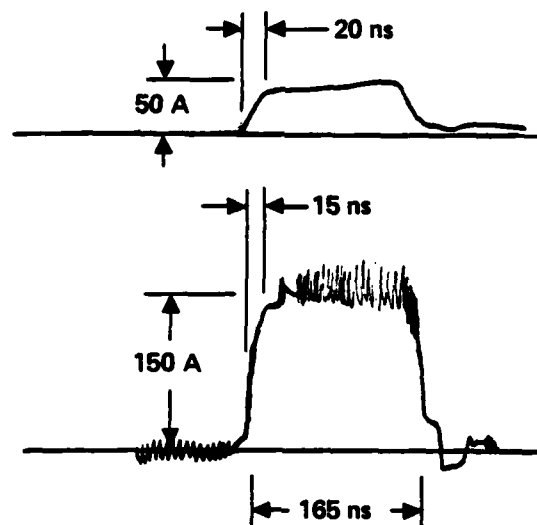Figure 3. Test model of crossatron switch.

Figure 4. High frequency response using a nega-
tively biased control grid. Pulse
is triggered when source current
reaches 200 A. The pulse shape is
determined by the network while the
amplitude depends on the voltage
(a) 1000 V (b) 2500 V.

16

Operating Characteristics

In the tetrode mode of operation, the rise time is a function of
the pressure, the switch inductance, the source current, and the control
grid pulse rise time. In the sequence, as shown in Figure 5, the anode
current first rises to the level of the source current in about the
same time as the control grid pulse rise time ($\sim$10 ns). The anode
current appears to saturate (after 9-10 ns) at the source current level.
After this time the anode current increases exponentially, as in a
conventional crossed field discharge, at a rate determined by the pres-
sure ($\overset{\circ}{I}\sim\Gamma I$, $\Gamma = f(P)$). Eventually, the rate of rise of current is limited
by the applied voltage divided by the inductance ($\overset{\circ}{I}\sim V/L$) and finally by
the circuit resistance.

The measured anode current rise is shown in Figure 6. It is a
superposition of 10 pulses measured at 30 kV at low repetition rate.
The jitter is less than 4 nsec and the 10-90% rise time is 28 nsec. The
100 A source current was considerably lower than the 1750 A peak anode
current and the effect of the low source current is just barely visible.

Alternate High Pressure Operation

Source grid currents of $\sim$60 kA may be impractical to achieve. In
that case, one would require a higher operating pressure in order to get
a short rise time. An example of the pressure dependence of the anode
fall time at 4 kV is shown in Figure 7. For this reason, the Paschen
breakdown limits of the crossatron as a function of pressure and the
anode voltage charging time are important. By pulse charging the
crossatron to 18 kV a few microseconds before triggering the grid, we
are able to temporarily exceed the dc Paschen limit without a breakdown,
even with preionization present. As shown in Figure 8, the pressure may
be increased 1.5X before complicating control problems are experienced.
An ultimate limit seems to exist at about 2X the dc limit. An important
consideration in burst (as opposed to CW or single shot) operation is
the dynamics of the adsorbed gases released from the electrodes at each
pulse. Gas evolution, and also acoustical wave propagation effects, may

17
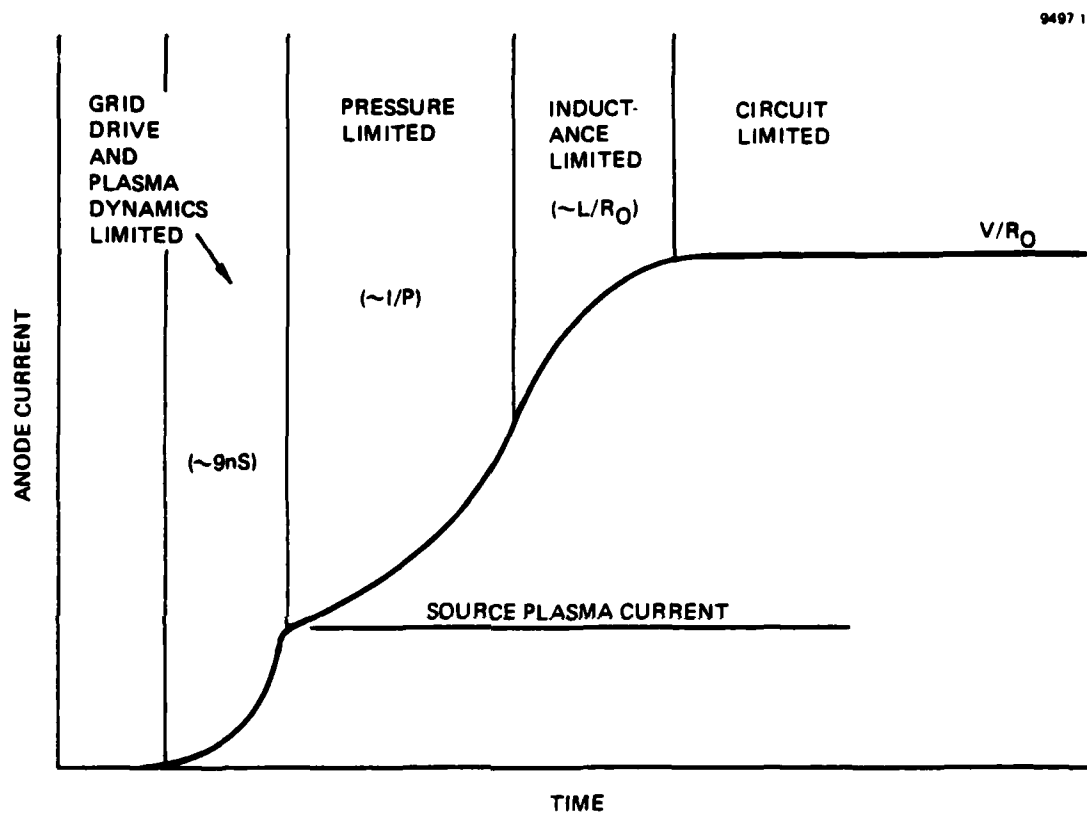
Figure 5. Schematic representation of anode current rise phases.
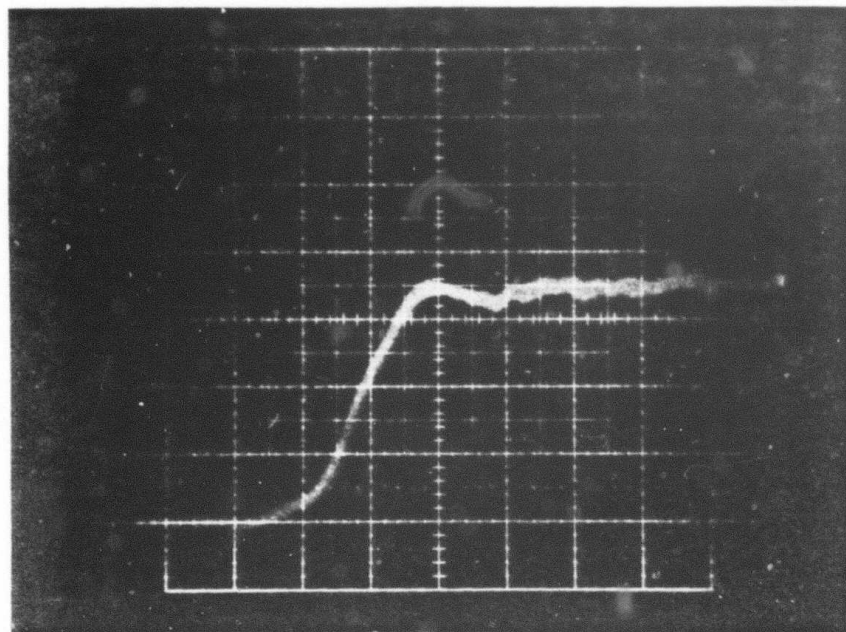
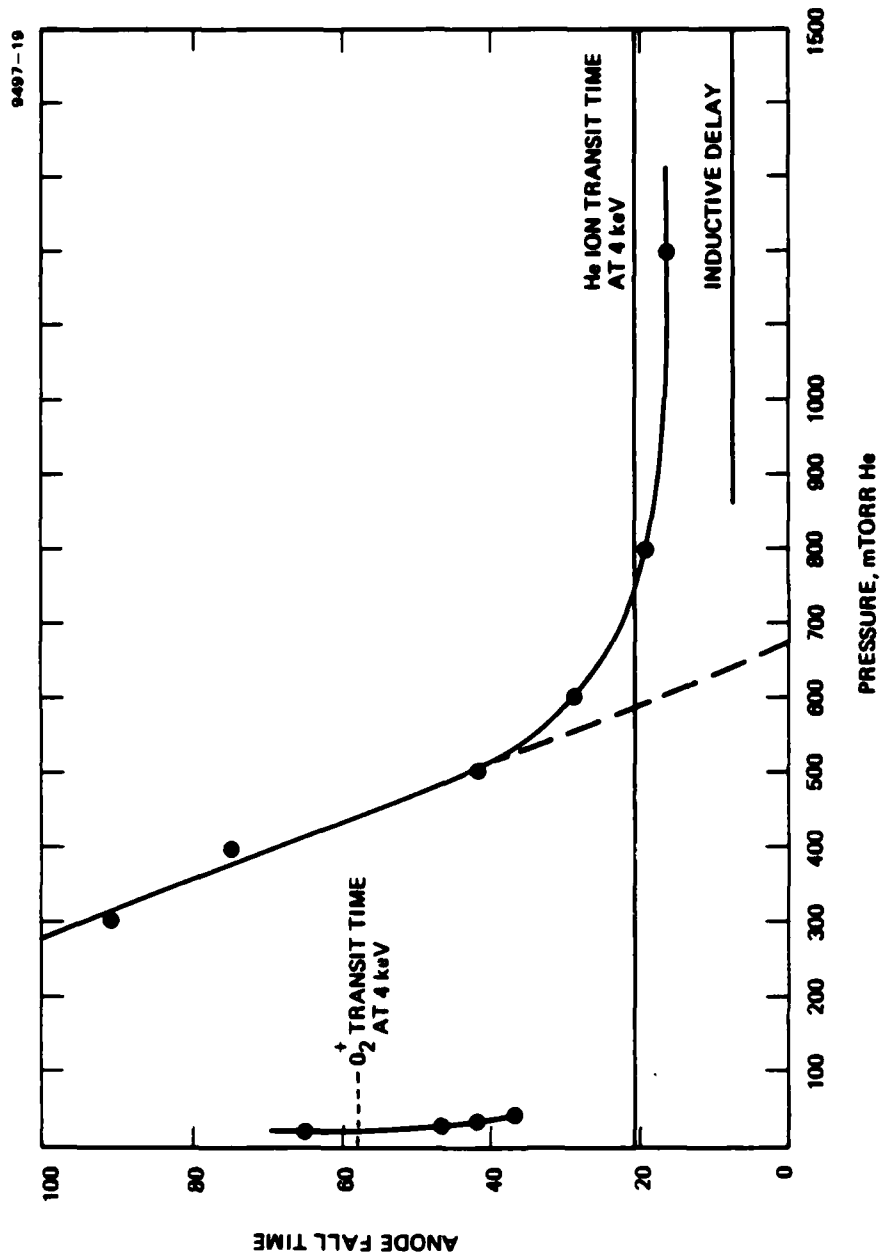Figure 6. Crossatron operation at 30 kV (ten superimposed pulses, P = 500 mTorr He).

Figure 7. Anode fall time versus pressure at 4 kV with low source current. Ion transit times and expected inductive delay time are shown for reference.
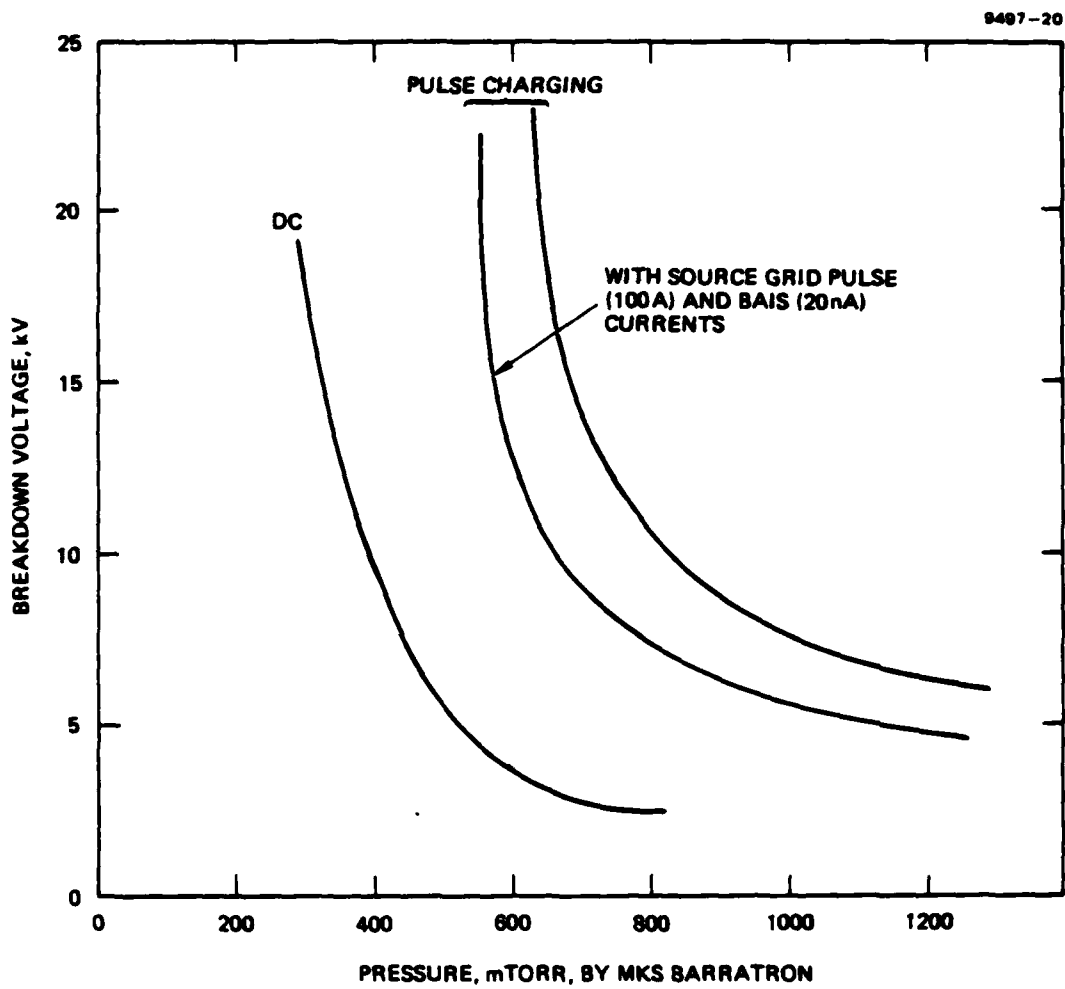
20

Figure 8. Pulse charge effect on Paschen breakdown (nonrepetitive).

21

lead to Paschen breakdown at lower voltage. Previously, we observed
and rectified similar effects in crossed field interrupters by proper
processing of the electrodes and by use of elevated operating tempera-
tures. If these results can be successfully scaled to 250 kV, it may be
possible to build a crossatron without the need for extra voltage grading
electrodes in the active region.

Crossatron Approach

The basic concept of the crossatron as a high repetition rate
switch has been verified. Empirical studies have confirmed early theo-
retical predictions of an intrinsically rapid current rise and a capa-
bility of operation at low jitter. High voltage operation has not yet
been achieved. The design and test of a suitable high voltage bushing
are necessary. Two basic approaches to a full power device exist.
First, the use of a relatively low voltage to obtain a $\sim$60 kA source
grid current just prior to the control grid trigger pulse may negate
the need for a high pressure and thus remove the Paschen breakdown
problem at HV. In order for this process to be energetically efficient,
the pulse length of the source current would need to be $\lesssim$1 μsec. To
avoid arcing in the source section, the surface area would need to be
$\sim$0.3 m^2. A design (Figure 1) incorporating these constraints along with
low inductance appears feasible. The advantage of this approach is that
the anode current rise times may be expected to be $\sim$10 nsec even with
a relatively low (i.e., Paschen breakdown safe) operating pressure. The
second approach uses a low source current, but requires a means of
improving the transient Paschen breakdown characteristics. It is pos-
sible that this may be achieved by minimizing the extent of absorbed
gases on electrode surfaces and by varying the electrode composition,
processing and temperature. The recovery control characteristics of the
crossatron at high pressure, due e.g. to acoustical wave propagation
also need to be determined in order to define optimized electrode geo-
metries. These approaches are expected to lead to a relatively small
device which would not require voltage gradient electrodes.

22

SECTION III

VACUUM SURFACE FLASHOVER SWITCH

Introduction

The vacuum surface flashover switch (VSFS) is a low pressure or vacuum device where conduction takes place in an arc or flashover along an insulator surface. The principle advantages of the VSFS are its projected short current rise time and rapid recovery. The operating principles for the VSFS are derived from the observation[6] that high voltage devices flashover at reduced voltage if the vacuum-metal-insulator triple point is not properly shielded. Thus, if the triple point is shielded from the high electric field (by a nearby grid or trigger electrode), the insulator will withstand a relatively high voltage. A positive voltage pulse is applied to the trigger electrode to close the switch. This results in field emission from the cathode electrode at the triple point. The hypothesis is that these field emitted electrons impact the insulator surface causing secondary electron emission, and this cascade effect causes an avalanche discharge with a high di/dt and a low voltage drop.[4] The insulator surface may be positively charged from the effects of secondary emission and may serve to neutralize the space charge. Also, gas may be evolved from the insulator surface, ionized, and serve to conduct current. Since this VSFS is a vacuum device, the plasma is assumed to quickly disperse after a current zero, and the voltage recovery should be adequate for high repetition rate operation. A diagram of a VSFS, used in preliminary experiments is shown in Figure 9.

Five different experimental VSFS's have been fabricated and evaluated. The following sections contain a discussion of these preliminary experimental results, and projected approaches for developing the VSFS into a device that meets the system requirements.
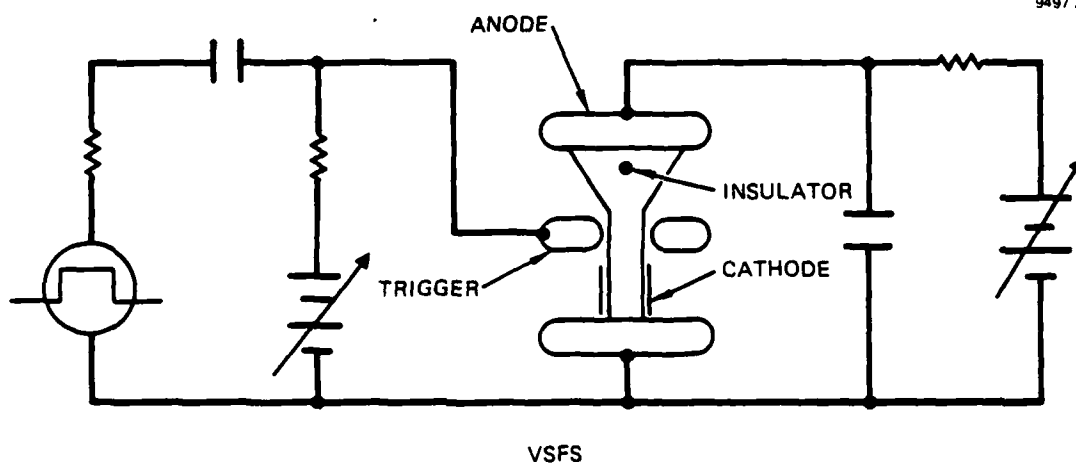
23

Figure 9. Test circuit for VSFS.

24

Experimental Results

Initial experiments were designed to measure the basic characteristics and to define the key problems of the VSFS. Ceramic (Al_2O_3) and plastics (polyethylene, polycarbonate, polyamide) with several different shapes were used as insulators. The original insulator shape was cylindrical and the cone shaped insulators were used to enhance electron bombardment of the insulator surface by the field emitted electrons from the cathode electrode.[6] Figure 10 shows these cylindrical and cone shaped insulator inserts along with the original VSFS geometry. Here, the cathode was in the form of a metal foil wrapped on the insulator and the trigger electrode was located at a slightly larger diameter.

The cathode material was tantalum; brass was used for the anode and copper was used for the trigger electrode. The VSFS were mounted in a glass vacuum container and continuously pumped with a turbo-molecular pumping system to a pressure $<10^{-5}$ Torr. The essential features of the test circuit are shown in Figure 9.

The cathode-anode breakdown voltage as a function of the bias (trigger) voltage for the nylon insulators is shown in Figure 11. Similar results were obtained with the other configurations and materials. There is a large variation in the breakdown voltage and, in addition, the breakdown voltage generally increases as the VSFS is used or conditioned. Typical anode and trigger voltages are shown in Figure 12 for the cylindrical ceramic insulator. On this time scale (10 µsec/div), the anode voltage falls abruptly and a trigger voltage of approximately 12.5 kV is required for an anode voltage of 25 kV. The arc appears to be confined to a localized region, but it does move from region to region for different switching pulses.

The switching results with the cone shaped Lexan (polycarbonate) and Nylon (polyamide) insulators are similar and typical anode fall and trigger voltages are shown in Figure 13. The anode current is shown in Figure 14. The anode waveshape is determined mainly by the test circuit capacitance and inductance. The anode fall and trigger voltage are shown

25

ANODE

TRIGGER

CATHODE

INSULATOR

1 cm

Figure 10. Test model VSFS and sample insulator inserts.
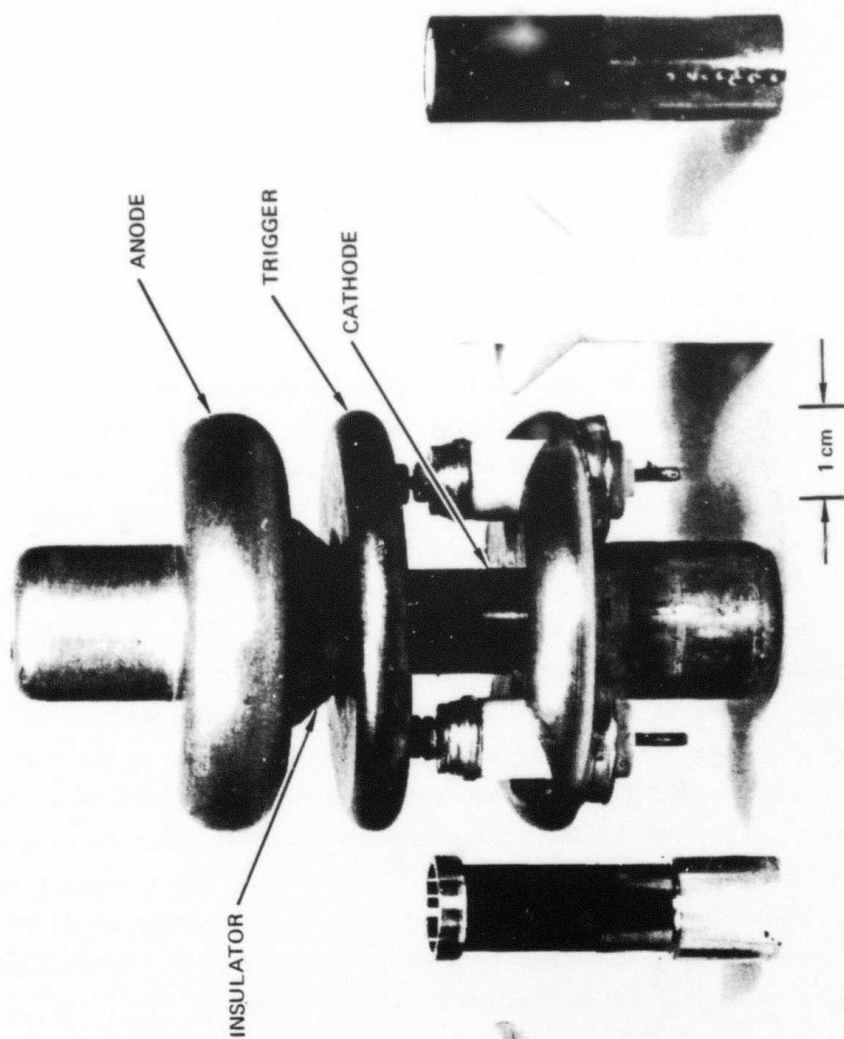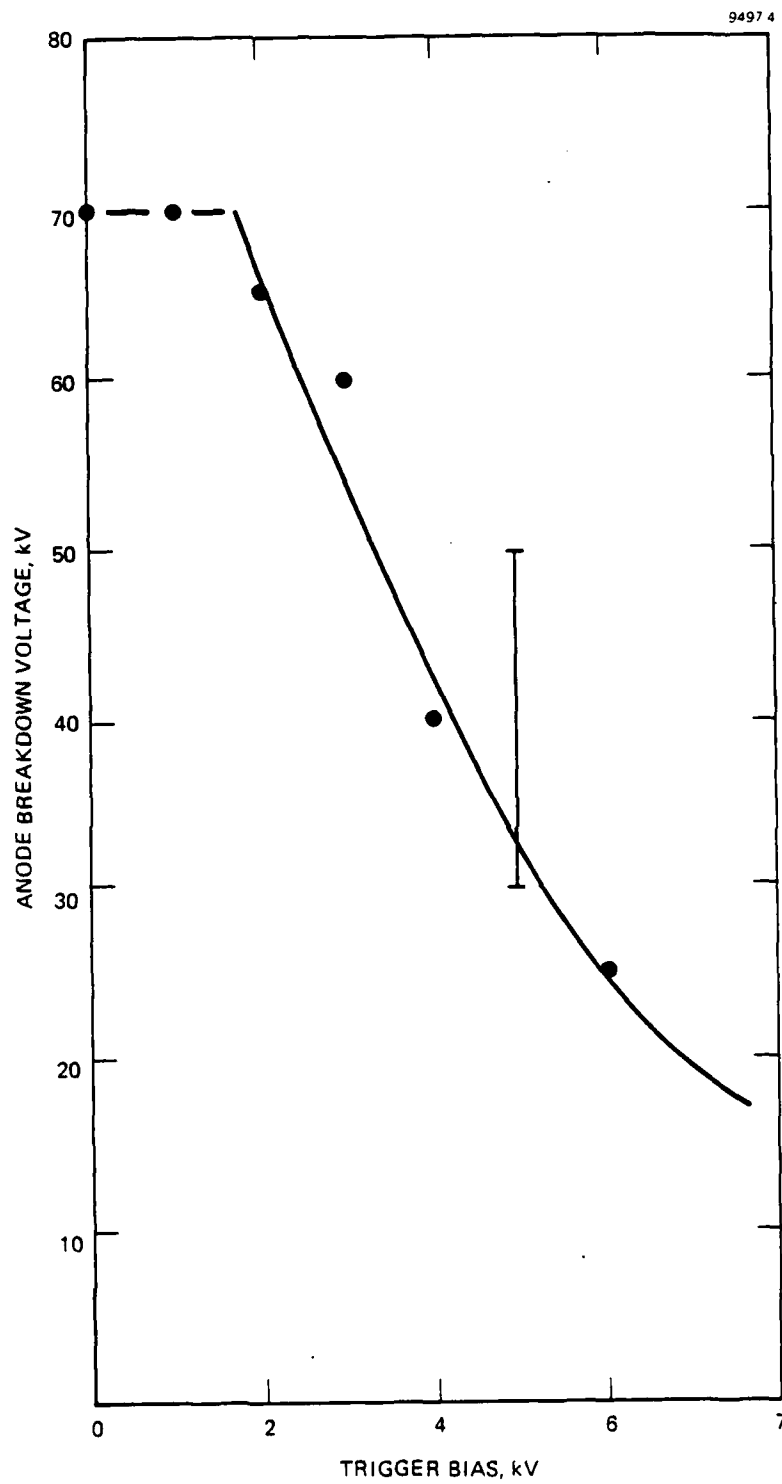
Figure 11. Cathode-anode breakdown voltage versus
trigger bias voltage.
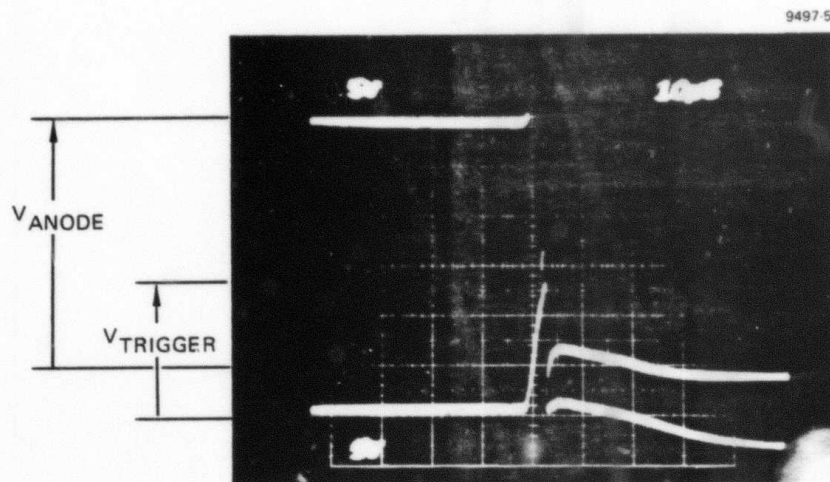
Figure 12.   Anode and trigger voltage (5 kV/D) versus time
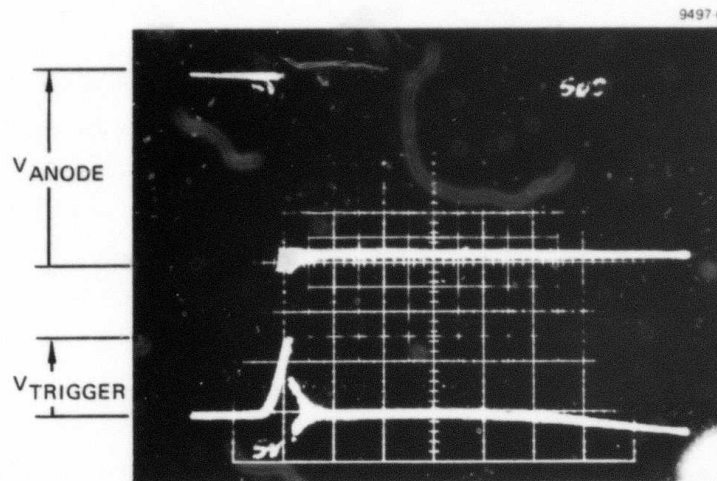   (10 μs/D) for ceramic insulator VSFS.

9497-6

Figure 13. Anode voltage (10 kV/D) and trigger volt-
age (5 kV/D) for cone shaped insulator
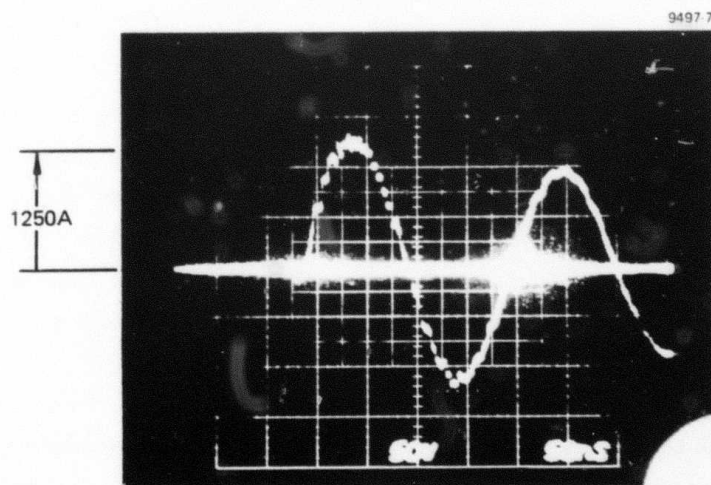VSFS, 5 μsec/D.

9497-7

Figure 14. Anode current (500 A/D) for VSFS,
50 nsec/D.

on a much faster time scale (20 nsec/D) in Figure 15. The anode fall
time measures approximately 12 nsec (10-90% points).

As these VSFS are used (conditioned), jitter increases and the
"firing" or switching becomes erratic. This is shown in Figure 16 with
the traces of anode and trigger voltages. The scope was set for alter-
nate sweeps so that each trace represents a separate switching operation.
Shown is a time variation or jitter between anode falls of ∿10 ns
and a failure of the VSFS to "fire" by the trigger voltage trace that
does not collapse.

Discussion of Results

The relevant switch requirements are high voltage (250 kV), high
current (40 kA), fast rise time and low jitter (∿1 ns), high repetition
rate (>1 kHz), trigger control, reliability, life, efficiency, and size
and cost.

The plastic insulator (Lexan & Nylon) VSFS were operated at an
anode voltage of 50 kV. The anode to trigger spacing was approximately
0.7 cm for a gradient of ∿70 kV/cm. Assuming a linear scaling by a fac-
tor of 5X, a 250 kV switch could require a spacing of ∿3.5 cm.

The currents conducted in the initial experiments (∿1 kA) caused
only minor erosion of the electrode and insulator surfaces. The ceramic
insulator was metal-coated after hundreds of switching operations, but
not to the extent that the switch was shorted out. After 100's of
operations the plastic insulators remained relatively free of coating
and developed a slight brownish coating at the ends and a glazed or fire
polished appearance in the center.

To this point, the test circuit, not the switch, has limited the
current to the ∿1 kA range. The anode voltage fall measures 15-20 ns.
Most of the anode current rise time can be attributed to the test
circuit, which has an anode-cathode loop inductance of ∿0.7 µH.
Although the exact conduction mechanism for the VSFS is not well
understood, it is not expected that times greater than a few nanoseconds
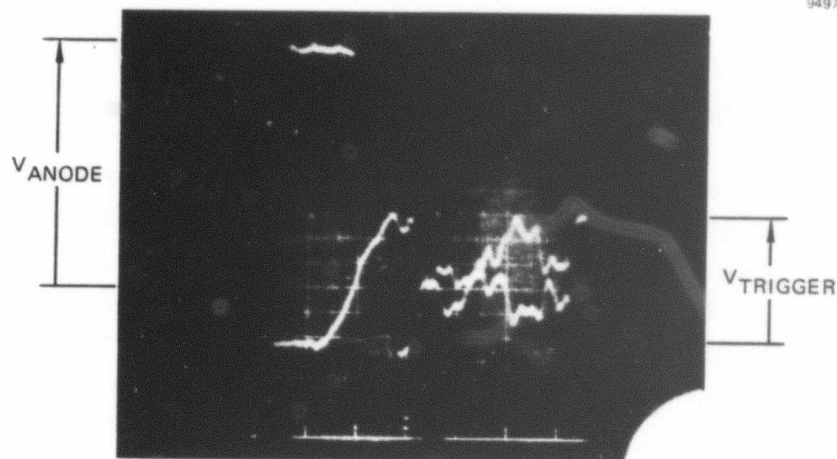
30

9497-8

Figure 15.   Anode voltage fall (10 kV/D) and trigger voltage
             (5 kV/D), at 20 nsec/D.

9497-9

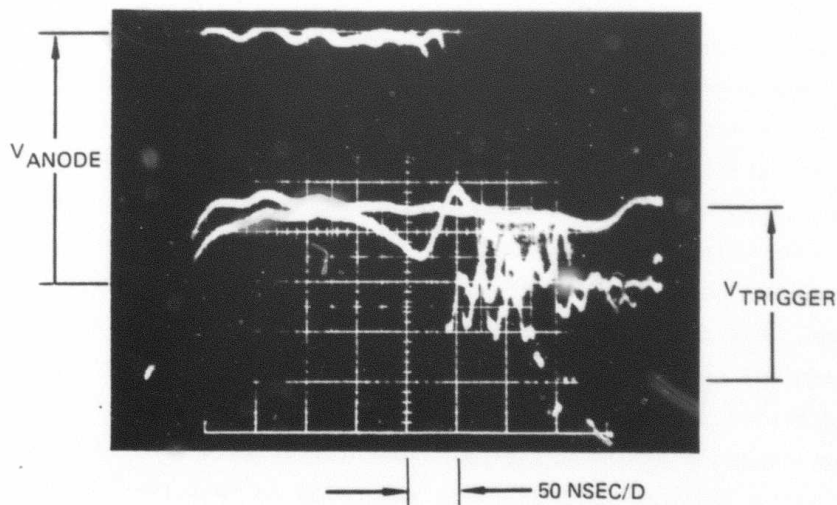50 NSEC/D

Figure 16.   Increase of jitter characteristics after condi-
             tioning. Anode and trigger voltages displayed
             on alternate sweeps. For one trace the VSFS did
             not "fire" — $V_{trigger}$ did not collapse.

are required for electron avalanche, but plasma generation by gas
evolution may require a longer time.

As seen from Figure 13, the anode voltage fall occurs as the
trigger voltage increases (to about 12 kV) and the jitter should be
reducible by increasing the trigger dV/dt. However, after switch opera-
tions of 100's of pulses, and for a trigger voltage of ∿17 kV, the anode
fall occurs during the flat or constant portion of the trigger pulse or,
in some cases, the anode fails to "fire."

The applied voltage recovery rates were low and no difficulties
were encountered with switch voltage recovery. Operated in purely the
electron avalanche mode, the VSFS is essentially a vacuum device and no
recovery problems are expected. However, gas evolution or fast recovery
measurements have not yet been made.

Triple Point Effects

The trigger control, reliability and life all appear to be inter-
related. The anode breakdown voltage as a function of the trigger bias
is changed with switch usage. This change is in the direction of higher
breakdown voltages. Also, the breakdown voltages are more variable;
i.e., spread over a larger range. Concurrently, an increased trigger
voltage is required, the jitter increases, and the reliability decreases.
Part of this variation is due to erosion of material at the triple point.
Figure 17 shows a photomicrograph of this erosion after the electrode
breakdown voltage had stabilized at a higher value. By using an auxil-
iary triple point field emitter to initiate the discharge, Figure 18,
we were able to isolate the sensitive trigger operation from the cathode
current and decrease erosion. An estimated electron current gain of 10^6 X
was achieved between the trigger and the cathode. However, the switch
jitter remained relatively high. This jitter is a central issue.

The efficiency appears to be very high in that the current is
determined by the test circuit, the switch voltage drop is not detect-
able on the same scale as the switching voltage is measured, and the
switch losses do not overheat the electrodes. To date, the switch per-
formances do not indicate that any size or cost problems should be
encountered.

32

9497-16

(A)

POTTING PLASTIC

TA CATHODE

NYLON INSULATOR

(B)

MODIFICATION

INSULATOR

METAL

(C)

TA CATHODE

TA CATHODE

NYLON INSULATOR

NYLON INSULATOR

ORIGINAL
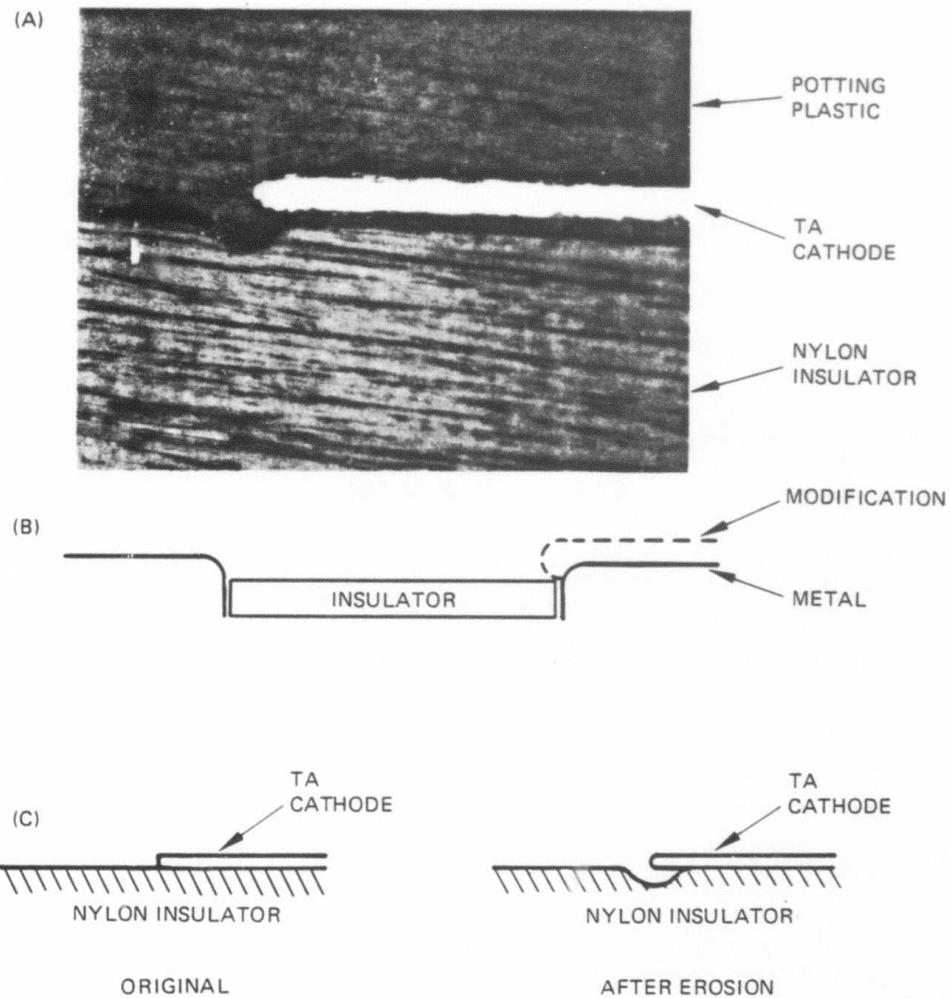
AFTER EROSION

Figure 17. (A) Photomicrograph of the erosion of the insulator at the triple point for a VSFS, (B) typical metal-ceramic insulator assembly and as modified to withstand higher voltage, and (C) schematic of the VSFS triple point before and after erosion.
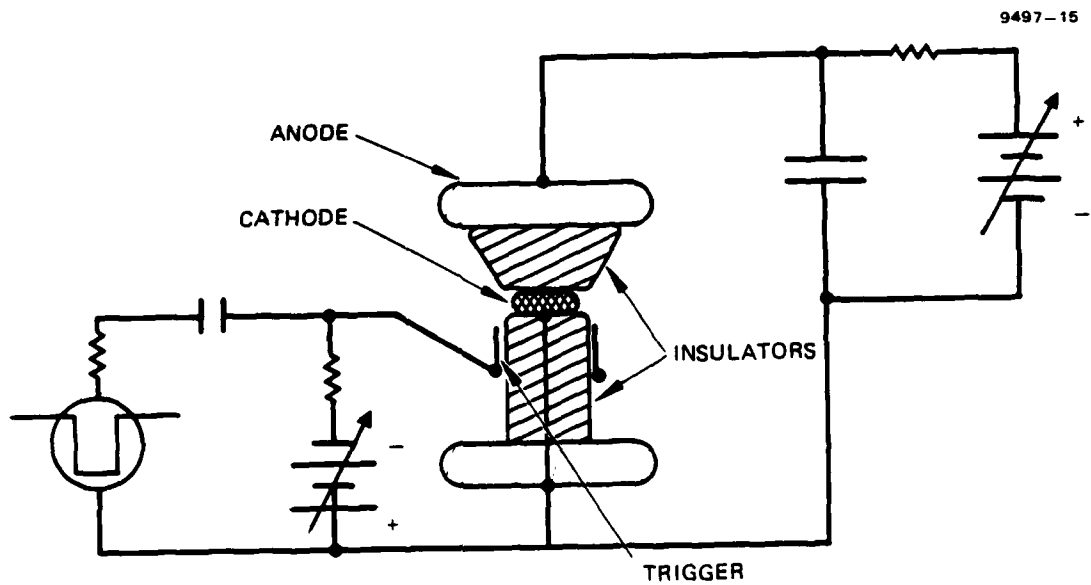
33

9497-15

ANODE

CATHODE

INSULATORS

TRIGGER

Figure 18. Auxiliary Triple Point Field Emitters VSFS and test circuit.

34

VSFS Approach Requirements

The switch jitter appears to be related to a conditioning effect, or the change in the breakdown voltage with operation. It is a key phenomenon which requires further study. Possible causal mechanisms in addition to the known triple point erosion effect include: (1) changes in the secondary emission coefficient of the insulator surface, (2) changes in the composition of desorbed gases from the surface, (3) erratic distortion of the field due to charging of the insulator, (4) a reduction in the field emission at the triple point due to a thin deposition of conductive material on the insulator, and (5) an increase of the cathode metal work function from contamination. Our data has been obtained under essentially dc conditions. Pulse charging is expected to remove some of the variability that we experienced. However, a reliable dc voltage holdoff is considered to be an indicator of the kind of reliability that is needed to operate a practical system composed of hundreds of switches.

For these reasons, means of determining and eliminating the causal mechanism for the conditioning effect are required in order to allow a reproducible surface charge distribution from pulse to pulse.

If the arc is continuously modifying the insulator surface, it may be possible to force the arc away from the surface with J x B forces. An investigation of arc location and behavior should be undertaken in relationship to various applied magnetic field geometries.

The VSFS anode-cathode circuit inductance masked the switch rise time characteristics but single channel formation may be a limiting factor when low inductance switches are constructed. Multiple (parallel) triggers or surface elements may need to be considered in order to distribute the arc over a large area and also to increase the switch reliability and life.

Additionally, the voltage recovery characteristics and VSFS operation under anode pulse charging conditions need to be determined.

SECTION IV

PRESSURIZED SPARK GAPS

Introduction

Basically, the rate of recovery of voltage in a pressurized spark-gap is controlled by a combination of: (1) nonequilibrium thermodynamic deionization, and (2) turbulent aerodynamic sweep-out of conductive arc remnants. If, at the time of reapplication of voltage, the ionization level is too high, the space charge distorts the electrostatic field locally and breakdowns occur[8,9,10,11,12]. Below we consider the issues of deionization, sweep-out, turbulence, frequency limits, drag losses, cavitation, shock formation and switch design approaches.

Deionization

The 50 nsec pulse length of the discharge current is too short for thermodynamic equilibrium. Following the arc there is a phase, (Δt_1), during which cooling, diffusion, and chemical reaction rates are high. This is followed by a second phase (Δt_2), during which the more stable forms of ions recombine. The details of these processes are complex and vary greatly with the gas composition, pressure, and current. Typically, the first phase lasts for $\Delta t_1 \sim 100$ usec[8] and may be affected by the pressure. The time scale for recombination is on the order of 1 to 10 msec[9,10,11]. It is shown, for example, in Ref 8 that the three-body recombination rates for

$$S_2^+ + F^- + F \longrightarrow \begin{cases} S_2 + F + F \\ SF + F + S \\ S_2 + F_2 \\ SF + SF \end{cases}$$
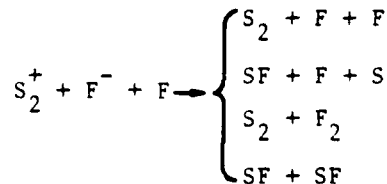
i.e., $r = 6.61 \times 10^{-20}(T)^{-5/2}$ [cm^6/sec]

37

dominate the recover characteristics of SF_6 during the recombination phase. In general, the ion density varies roughly as

$$\dot{n} \sim -r n^2 n_0$$

or

$$n(t) = \frac{n(\Delta t_1)}{1 + r\, n_0 n(\Delta t_1) \cdot (t - \Delta t_1)} \quad , \quad t > \Delta t_1$$

where n_0 is the neutral gas density in the channel.

The gas temperature is high ($\sim 2000^\circ K$ for $P = 1$ atm) at the start of the second phase. Thus, the neutral density is lower by a substantial factor (~ 7) from the room temperature gas outside of the arc region. This is an arc induced cavitation effect which must also be accounted for when the dielectric strength of the gas is considered later.

We define the deionization recovery time, $t_r = \Delta t_1 + \Delta t_2$, to be given by the time at which the ion density space charge falls below the space charge distortion limit

$$n(t_r) \leq \varepsilon E/e\ell \sim 2 \times 10^{10}\ cm^{-3}.$$

Based on this model, the SF_6 gas pressure required to achieve a 1 ms recovery is about 7 atm. This increases to about 70 atm for $t_r \sim 100\ \mu sec$. SF_6 actually liquifies at about 20 atm, but other gas mixtures (e.g., $Ar + H_2$)[13] may conceivably have similar extrapolated recovery properties at such high pressures.

Aerodynamic Sweep-Out

The aerodynamic sweep-out of spent gases from the sparkgap is conventionally used to compensate for the slow deionization time of the arc channel. During this sweep-out the arc remnants are physically removed from the electrode region, and the are remnants are cooled and diffused by small scale turbulence.

Other undesirable and often unrecognized effects are that large scale turbulence statistically returns conductive gases upstream, and density reductions form at obstacles or at constriction in the flow pattern.

The operating frequency, f, of the switch is limited by the flow velocity, v, and the characteristic size of the high electric field region, ℓ, according to

$$f < v/\ell \tag{1}$$

Ignoring any design improvements necessary to avoid cavitation, the velocity is limited to sonic speeds (v<c), where $c = \sqrt{\gamma RT/M}$. Therefore, in order to increase f, it is important to keep ℓ as small as possible. This, in turn, requires the gas density, η_o, to be as high as possible in order to achieve a high dielectric strength. From Ref. 14, we find that

$$E = \frac{V}{\ell} < K_1 \left(24.2 \cdot \eta_o + 6.08 \sqrt{\frac{\eta_o}{\ell}} \right) \times 10^3 \text{ V/cm} \tag{2}$$

where η_o is in reduced units.

This complicated expression assumes a field enhancement factor of unity and reduces for V = 250 kV to

$$\eta_o = K/\ell . \tag{3}$$

where ℓ is in cm and K = 8.7 for N_2 and 3.0 to 3.65 for SF_6. The result for f is then

$$f < \left(\frac{c}{K} \right) \eta_o . \tag{4}$$

Due to the faster sound speed of N_2, which compensates for the K value, $c/K \sim 3.8 \times 10^3$ for either gas. This crude approximation implies that $f = 10^4$ Hz would require a pressure of about 4 atm, a gap size on the

39

order of 1 to 3 cm and $v \sim c$. Any pressure fall in the flow or thermally induced cavitation would reqire an increase in the source pressure. This correction factor must be determined but it is likely to be significant.

Drag Losses

Following Ref. 15 and 16, the critical Reynold's numbers R_C for stable flow in channels and concentric cylinders are 660 and 1900 respectively. In our case $R \equiv v \cdot \ell/\nu \sim 2.1 \times 10^6$ and the flow is turbulent, (where ν is the kinematical viscosity). Under these circumstances, the drag forces may be estimated by

$$\text{drag} \sim \frac{\mu v}{\ell} \cdot A \cdot R/Rc \quad (R > Rc) \tag{5}$$

where the dynamical viscosity $\mu = \nu \cdot \eta_o$ is pressure independent.

The power loss is given by

$$\text{power loss} = v \cdot \text{drag} + \text{enthalpy loss}$$

$$\sim \frac{\eta_o v^3 A}{Rc} + \left(\frac{\gamma}{\gamma-1}\right) \; P \cdot \ell^3 \cdot f$$

$$\sim 11 \cdot A + 283 \times 10^3, \text{ (Watts)}$$

where A is the surface area of the flow system in cm^2. This calculation ignores compressor efficiencies and assumes 5 atm of N_2.

During a ten pulse switching burst at 10 kHz, delivering 2.5 kJ to a load, the gas (N_2) would travel only about 30 cm, have an enthalpy of about 280 J and lose by drag forces about 3.4 kJ. Obviously, continuous operation is not practical. Pneumatic or chemical energy storage may be the most efficient means of achieving such flows on a pulsed basis. If "ready-state" operation is required, then the gas should be recirculated with the compressor as near to the switch as possible.

Cavitation

We have available a body of proprietary data detailing the interruption of arcs in pressurized electro-mechanical switches. These switches have made use of high pressure gas blasters to drive the arcs and remnant gas away from the electrodes. These data were obtained on operating devices using: pressure, current and voltage transducers and other techniques, such as high speed image converter camera, Shlieren, and shadow graph photography. These were confirmed by the use of experimental fluid models and computer simulations of the flow patterns.

The sequence of events, relevant to pressurized spark gaps, is as follows:

(a) A high pressure source is connected through a constricting fast electro-mechanical valve (dashed outline, Figure 19) into a section at lower pressure. The initial density profile[17] is shown as curve (0) in Figure 19.

(b) The valve is opened, the flow passes through the constriction, and rapidly establishes the density at that point to be approximately half the value of the source pressure. Past the constriction, the gas expands rapidly pushing the gas ahead of it out of the way. This forms a rarefaction-wave curve (1), which travels downstream until a stable Mach-disk forms, curves (8), (9), and (10). The steady state density falls below the initial density just beyond the edge of the constriction and falls to a very low value just ahead of the Mach disk.

It should be evident that the dielectric strength of such a flow pattern will be correspondingly very low in the expanding section, and the location of electrodes in or near such a region is to be avoided.

Shock Formation

The electrode edges affect the flow pattern. Typically, standing shockwaves form at the leading edges, bend into the flow, intersect at the center, and return to the electrodes downstream. A variety of pressure jumps are possible across the intersecting boundaries and arcs are commonly observed to follow the intersecting counters. Figure 20a

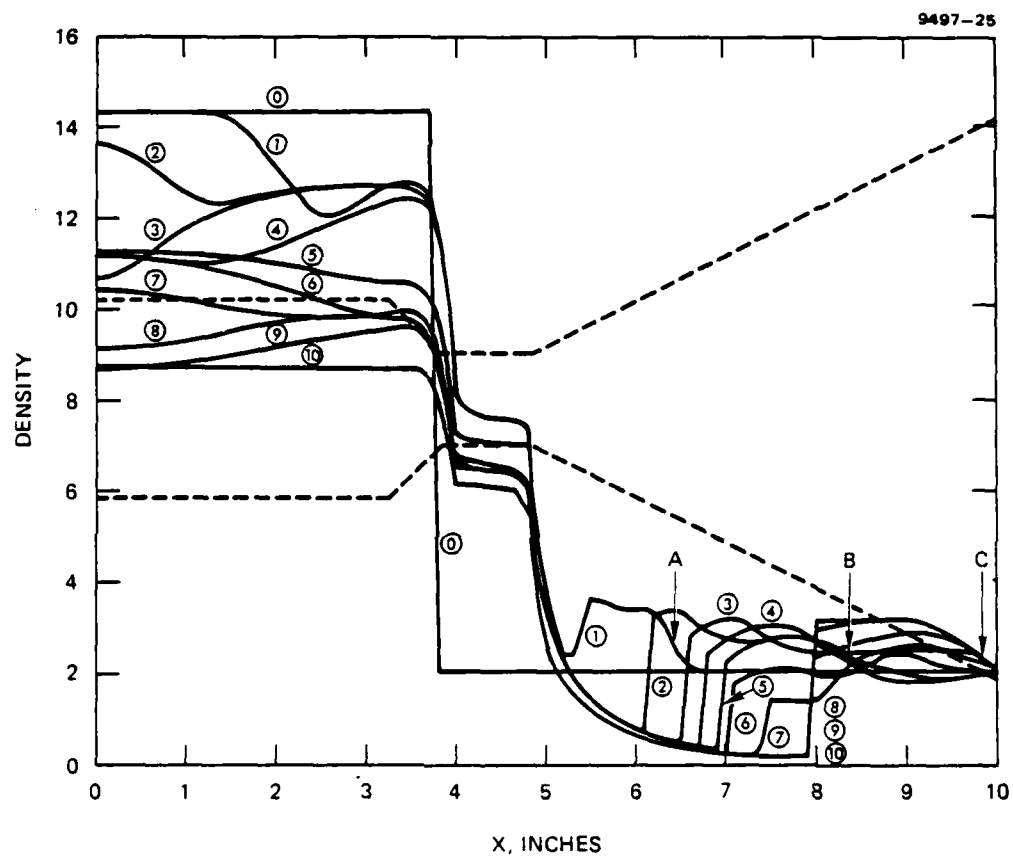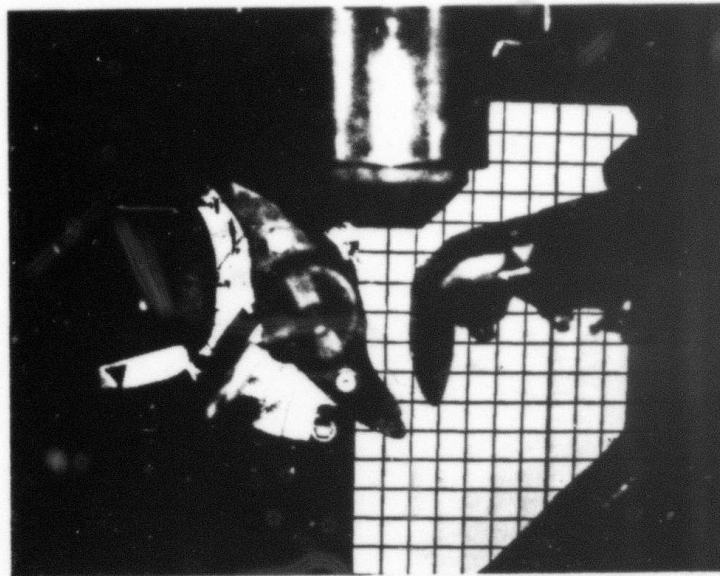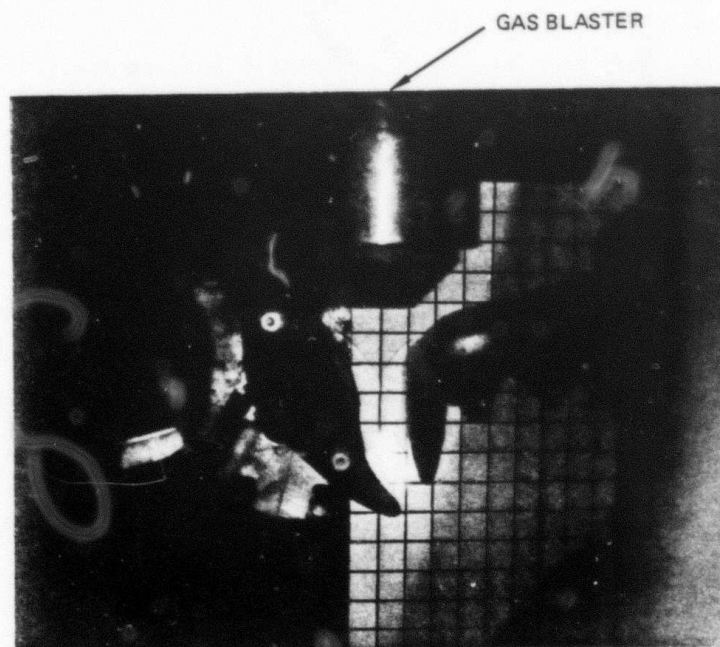Figure 19. Cavitation in a high pressure flow.

a

V = 0

GAS BLASTER

b

V = 45kV

Figure 20. Shadowgraph representation of enhanced arc propaga-
tion along shock structures in high pressure flows.
Grid size = 1/2 in. $P_{blasted}$ = 200 psi.

43

shows a shadow graph of the shock wave structure in a typical flow pattern.[20] The 200 psi SF_6 gas blast system is at the top and the flow takes place between two shaped electrodes into 1 atm SF_6 + N_2 at the bottom. Figure 20b shows approximately the same flow pattern with ∿45 kV applied to the 0.7" gap. Here the gas broke down and the arc followed the intersecting shock wave with a net arc path about 1.5 " long. Obviously this mechanism has serious implications to any HV system when strong flows exist.

Turbulence

Turbulence has important desirable and undesirable effects. Thermal cooling of the arc channel may be accelerated by turbulence. The effect of the turbulence is to increase the diffusion rates and spread the channel out. Small scale turbulence may be sufficient for these purposes and is therefore desirable. Locations where the flow stagnates must be cleared by turbulent flow. This is a statistical process which requires large scale turbulence to be effective, but has the undesirable side effects outlined below.

Typically the flow is characterized by an average flow field and a turbulent velocity flow field whose root-mean-squares are comparable. The turbulent flow is well defined on an instantaneous basis. This means that vortices are present which have reduced gas densities at their cores and which distort the original arc channel shape as it is swept down stream. Statistically, part of the conductive path may also be carried back up stream. Hence, a contorted but conductive path sometimes remains in the neighborhood of the electrodes for a time exceeding 100 us.

It is therefore necessary to control the scale of the turbulence, to avoid cavitation, and to eliminate regions of stagnant flow.

Pressurized Sparkgap Approach

Several other issues exist, (such as the stress loading of feed-through bushings, and the effects the propagation of acoustical waves

44

on the dielectric gas) but the increase of the recombination and cooling
rates by a judicious use of gas combinations at very high pressures
could conceivably be made the basis for the improvement of pressurized
spark gaps. This appears to be a complex and difficult task.

In order to increase the overall energy efficiency, it might be
practical to use relatively small self-contained units filled with high
pressure gases. These might for example be operated by synchronous
5 hp motors which would spin insulating impellers within the switch
cavity in order to reduce drag forces and start up times. Data for
voltage hold off and recovery times at high pressure are needed as
a function of gas composition.

In order to avoid rarefaction waves, cavitation, large scale
turbulence and stagnant flow, means of achieving a smooth interfacing
of the electrodes into a carefully designed flow channel are required.

SECTION V

THEORETICAL MODEL

1. Introduction

The behavior of the boundary of a plasma in the presence of a high applied electric is fundamentally important to the switching behavior of low pressure or vacuum devices. This section deals with an idealized plasma-vacuum boundary (Figure 21) which is presumed to have been held in place by a transparent but negatively biased grid electrode. When the grid is electrically removed, the plasma is free to expand into the right hand region where the electric field due to the anode extracts electrons. Space charge effects are dominant near the plasma boundary and the potential, ϕ, falls to a minimum value ϕ_m at a point X_m outside the plasma. At the plasma densities of interest, $n_o \approx 10^{14}$ cm^{-3}, the electron flux to the boundary J_o is about 10^5 A/cm^2 at an electron temperature of Te $\approx$ 10 eV. This flux is well above the initial space charge limited current density which is regulated by ϕ_m causing all electrons with energies less than about 90 eV to be reflected.

Ions are accelerated into the potential well. As sufficient numbers reach X_m, the electronic space charge is neutralized and the minimum position moves toward the anode.[21] The moving potential results in a collective acceleration of ions to energies higher than $|e\phi_m|$, which in turn is much higher than the electron temperature.

As with other gases, the collisional processes for He$^+$ in He are dominated by charge exchange. But the relatively high ionization potential of He results in a lower charge exchange cross section and longer mean free path. In Figure 22 we show the mean path for ions in a background pressure of 30 mTorr as deduced from Ref. 18. The solid lines are for He$^+$ in He and for H$^+$ in H. Also shown as dotted lines are representative positions of a He ion as a function of velocity when exposed to a constant electric field. Obviously the mean free path of 1.2 to 2.2 cm is on the order of, or slightly shorter than, the
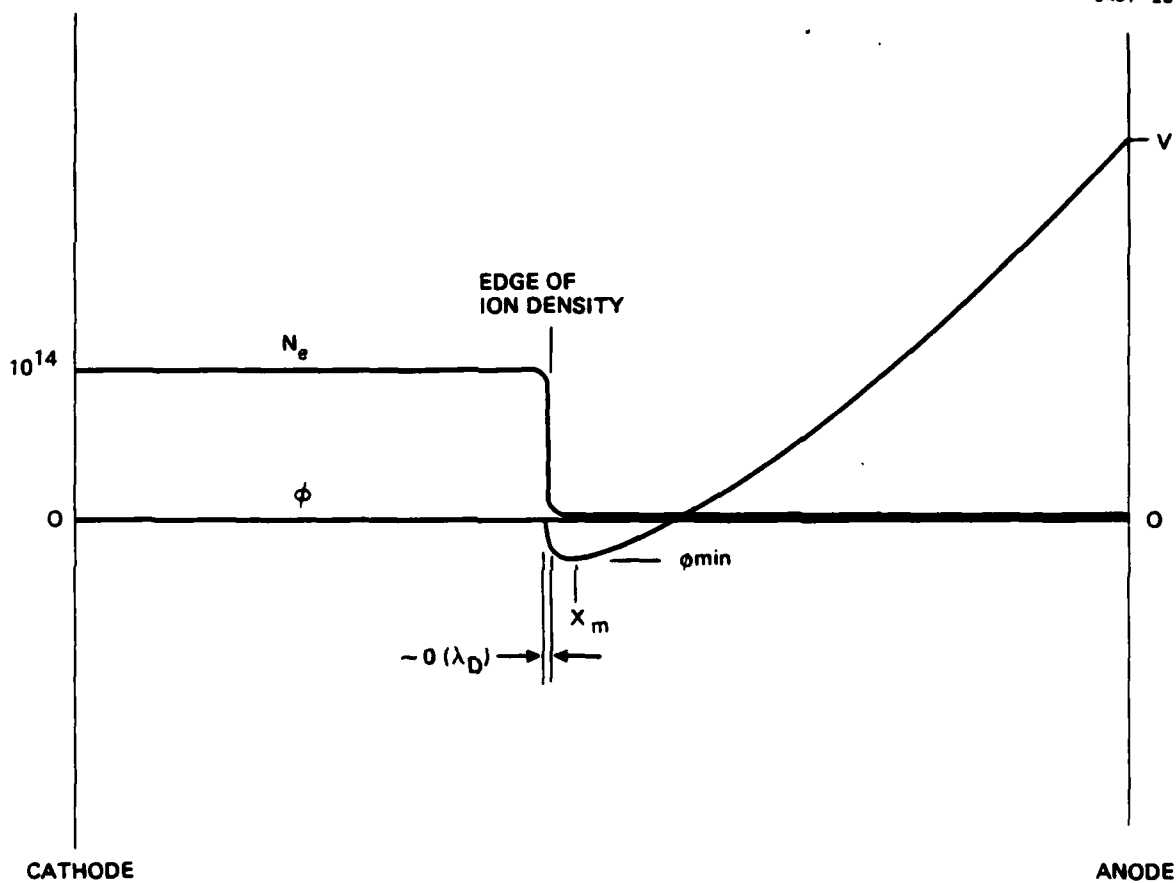
Figure 21. Initial electron density and potential configuration.
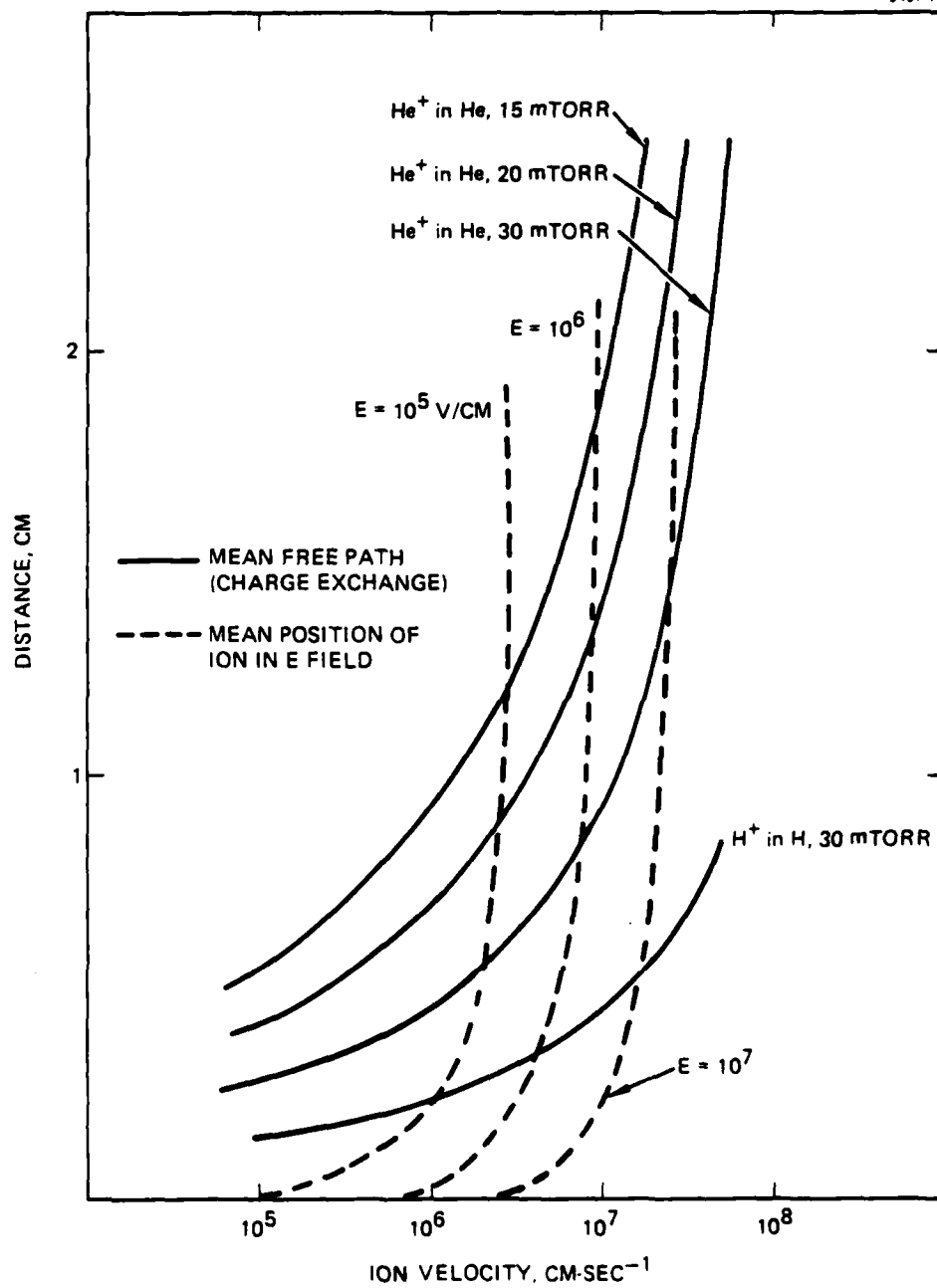
Figure 22. Mean free paths and mean position of an ion as a function of ion velocity and pressure.

dimensions of a projected crossatron switch (2 to 4 cm) over a broad range of anticipated electric fields. Thus we shall treat the ions as collisionless.

We have analyzed the plasma behavior both by analytical approximations and by computer simulations using a Vasov's Equation model for the propagation of ions in the self consistent electric field generated as a result of the motion of electrons. The electron flow is treated as being more rapid than the ion response time.

2. Analytical Model

We assume that a minimum potential, ϕ_m, exists somewhere between the plasma (at zero potential) and the anode (at V). Electrons with energies lower than $-e\phi_m$ are reflected from this minimum and returned to the plasma. Consequently, the space charge limited electron current that reaches the anode, J, is determined by the thermal flux of electrons in the plasma with energies above $-e\phi_m$ in the direction of the anode. This is given by

$$
J = en_o \int_{\sqrt{\frac{2e|\phi_m|}{m_e}}}^{\infty} v \frac{e^{-\frac{mv^2}{2kTe}}}{\sqrt{\frac{2\pi kT}{m_e}}} dv = en_o \sqrt{\frac{kT}{2\pi m_e}} \, e^{\frac{e\phi_m}{kT}} \tag{7}
$$

$$
= J_o \, e^{\frac{e\phi_m}{kT}} \quad \text{where } J_o = en_o \sqrt{\frac{kT}{2\pi m_e}} \tag{8}
$$

This may be inverted to yield

$$
\frac{e\phi_m}{kT} = \ln J/J_o \tag{9}
$$

50

The electron phase space density in the region where the potential varies must obey

$$\overset{\circ}{f}_e + v \cdot \frac{\partial f_e}{\partial \chi} + \frac{\nabla \phi}{m_e} \frac{\partial f_e}{\partial v} = 0 \qquad (10)$$

Since we assume the ions to be essentially at rest relative to the electrons we look for the steady state solution $\overset{\circ}{f}_e = 0$ or

$$f_e = f_e \left(\frac{mv^2}{2} - e\phi\right) \qquad (11)$$

This solution does not need to be continuous across boundaries where $\nabla\phi = 0$, and the analysis is complicated by the presence of the lowest intermediate potential minimum ϕ_i between the plasma and a position, x. The electron density distribution $n_e(x)$ is obtained by using a Maxwellian source function for f_e and integrating only over regions in velocity space where electrons may be present due to streaming from the $x = -\infty$ boundary. Thus:

$$n_e(\phi) = C \left[\int_{-\sqrt{\frac{2e}{m}(\phi-\phi_m)}}^{\infty} e^{-\left(\frac{mv^2}{2} - e\phi\right)/kT} \, dv - \int_{-\sqrt{\frac{2e}{m}(\phi-\phi_i)}}^{\sqrt{\frac{2e}{m}(\phi-\phi_i)}} e^{-\left(\frac{mv^2}{2} - e\phi\right)/kT} \, dv \right] \qquad (12)$$

To a high degree of accuracy the error function integrals in Eq. 12 may be approximated[19] to yield

$$n_e = n_o \left[\frac{e^{\frac{e\phi_i}{kT}}\left(\sqrt{\frac{e}{kT}(\phi-\phi_i)+\frac{4}{\pi}} - \sqrt{\frac{e}{kT}(\phi-\phi_i)}\right) - \frac{1}{2} e^{\frac{e\phi_m}{kT}}\left(\sqrt{\frac{e}{kT}(\phi-\phi_m)+\frac{4}{\pi}} - \sqrt{\frac{e}{kT}(\phi-\phi_m)}\right)}{\sqrt{4/\pi} - \frac{1}{2} e^{\frac{e\phi_m}{kT}} \sqrt{-\frac{e\phi_m}{kT}+\frac{4}{\pi}} - \sqrt{-\frac{e\phi_m}{kT}}} \right] \qquad (13)$$

51

where $\phi \geq \phi_i \geq \phi_m$.

The potential must then obey the nonlinear Poisson's equation

$$\nabla^2 \phi = \frac{\varepsilon}{e} \left(n_e(\phi) - n_i(x) \right) \qquad (14)$$

For the present we treat the ions as being a cold fluid satisfying the time dependent equations

$$\overset{\circ}{n}_i + \nabla (n_i v_i) = 0$$

$$\overset{\circ}{v}_i + \nabla \left(\frac{v_i^2}{2} + \frac{e\phi}{m_i} \right) = 0 \qquad (15)$$

In the falling region of the potential the above equations have a solution given by

$$n_i = n_o e^{-\frac{x}{v_o t}} \qquad (a)$$

$$v_i = v_o + x/t \qquad (b) \qquad (16)$$

$$\phi = -\frac{kTe}{e} \frac{x}{v_o t} \qquad (c)$$

where $v_o \equiv \sqrt{\frac{kTe}{m_i}}$. (This behavior is borne out by simulations to be of a limiting character in the falling region.) The characteristic velocity v_o is equivalent to an ion with half the electron thermal energy. By eliminating x/t from Eq. 16b and 16c it follows that the

52

collective mode of acceleration results in ion energies at a location $0 < x < x_m$ given by

$$\frac{m_i v_i^2}{2} = \frac{kTe}{2}\left(1 + |\frac{e\phi}{kTe}|\right)^2 = \frac{kTe}{2}\left(1 + \ln J_o/J\right)^2 \tag{17}$$

It should be noted that the energy source being tapped here is the plasma electron thermal energy which is finite and cannot maintain this condition indefinitely. Nevertheless, only a small fraction of the plasma ions need to be accelerated into the vacuum in order to cancel enough of the electronic space charge to produce a high anode current. This appears to be energetically self consistent for reasonable plasma volumes.

Beyond the minimum potential the potential eventually exceeds any of the thermal particle energies and we may assume a Child's law behavior for the current density[21]

$$J = KV^{3/2}\bigg/\left(d - (\Delta x + x_m)\right)^2 \tag{18}$$

where $K = 2.33 \times 10^{-6}$ (mks) and d is the initial grid to anode spacing. Since the minimum may be very flat we must treat $(\Delta x + x_m)$ as being the location where the ion density is no longer sufficient to influence the potential, see Figure 23.

In the neighborhood of x_m Eq. 14 reduces to

$$\nabla^2 \phi = \frac{\varepsilon}{e}\left(\frac{n_o\, e^{\frac{e\phi_m}{kT}}}{2} - n_i(x_m)\right) \tag{19}$$

If the ion density averages to be

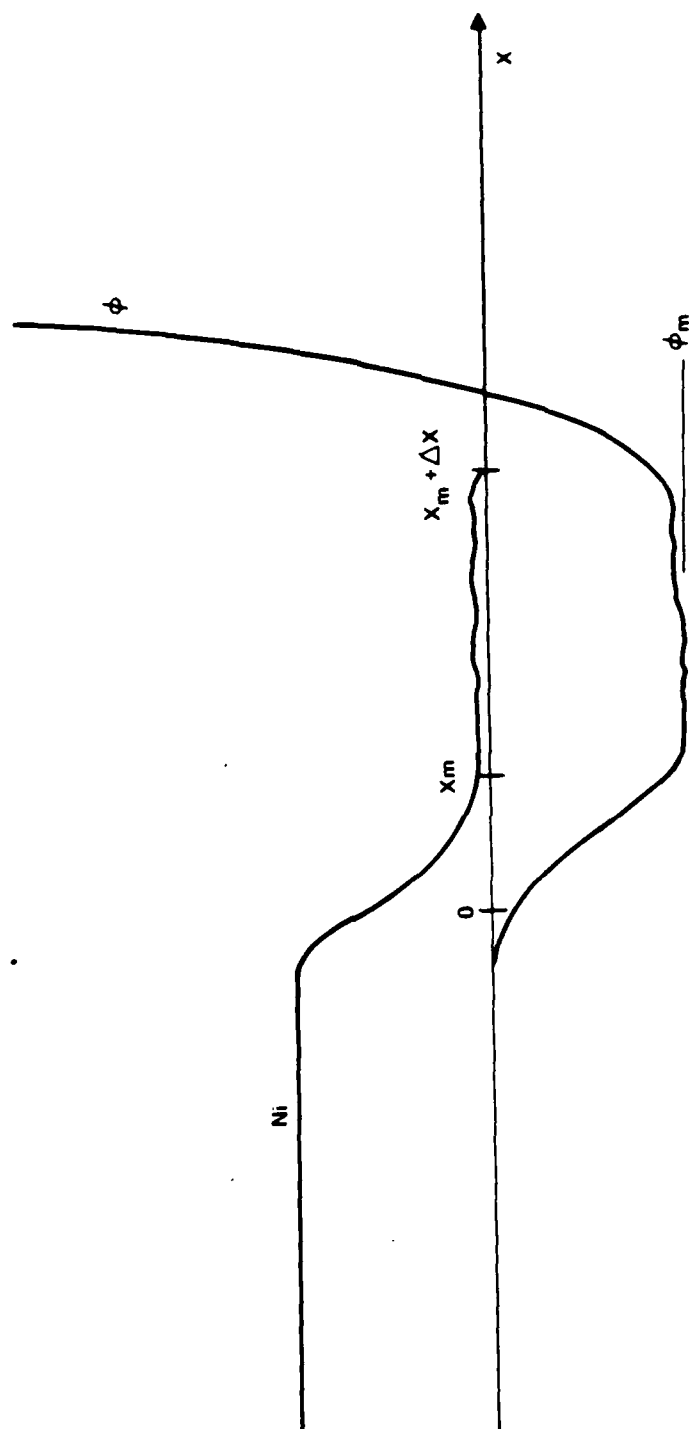$$n_i(\overline{x_m}) \sim \frac{n_o}{2} J/J_o \tag{20}$$

9497 21

Figure 23. Ion density and potential (schematic) after ions have reached the potential minimum region.

54

Then $t \approx t_m$, and the ions are free to drift.

The distance Δx over which this may be true is estimated by computing the number of ions accelerated past the minimum ($x_m = - v_o t \, e\phi_m/kT$) via Eq. 16:

$$N = \int_{x_m}^{\infty} n_i \, dx = n_o \, v_o t \, J/J_o \tag{21}$$

Dividing N by Δx yields the **mean density**

$$n_i \overline{(x_m)} = \frac{N}{\Delta x} \tag{22}$$

or from (20)
$$\Delta x = \frac{2J_o}{Jn_o} \, \frac{n_o \, v_o t \, J}{J_o} = 2 \, v_o t \; . \tag{23}$$

Thus the effective edge of the ionic space charge is at

$$\Delta x + x_m = v_o t \, (2 + \ln J_o/J) \tag{24}$$

and

$$J = \frac{KV^{3/2}}{\left(d - v_o t \left(2 + \ln \dfrac{J_o}{J} \right) \right)^2} \tag{25}$$

In terms of the initial value of $J = J_1 = KV^{3/2}/d^2$ we have finally

$$J = \frac{J_1}{\left(1 - \dfrac{v_o t}{d} \left(2 + \ln \dfrac{J_o}{J} \right) \right)^2} \tag{26}$$

$$J_1 \cdot J \cdot J_s \cdot J_o \; .$$

55

This function has been plotted in Figures 24 and 25 for several values of T_e, d and n_o. In order to reduce the current rise time it is advantageous to increase T_e and n_o (i.e., source current) while keeping the electrode spacing at a minimum.

These solutions have a maximal logarithmic rate of rise near $J = e^{-2} J_o$. This level is probably not attainable since the model breaks down altogether if the anode current exceeds the source current. However, current rise times of 10 to 20 ns seem practical if $J \leq 100A/cm^2$.

Other estimates of the current may be based on setting $\overset{o}{x}_m = v_m(x_m)$. These yield somewhat flatter base curves with more rapid rises. It is also apparent that oscillations of the ions will take place in the potential well causing the current to oscillate at a frequency which increases with J. It is not known if these effects are tractable analytically but the following simulation model is intrinsically capable of tracking the ions in the well.

3. Computer Model

The computer simulation model follows the ion density distribution in phase space using Eqns. 13 and 14 and the ion version of Eqn. 10. Since the equations are highly nonlinear small errors (numerical, or in the initial conditions) grow away from o as e^{x/λ_D} where λ_D is the Debye length. Thus 17 digits of accuracy will be lost in calculating for only 40 λ_D. We have found that the interesting regions of the plasma are larger than this in extent. By matching "asymptotic" solutions together every ~ 28 λ_D we have been able to maintain about 6 digits of accuracy in the calculated potential over a range of several hundred λ_D.

Figure 26 shows the ion phase space density at T = 4 ns starting with $n_o = 10^{20}$ m^{-3}.

Figure 27 shows the progression of the ion density distribution and the potential in the front of the plasma as a function of time. It is likely that the spatial oscillations were a result of the finite grid
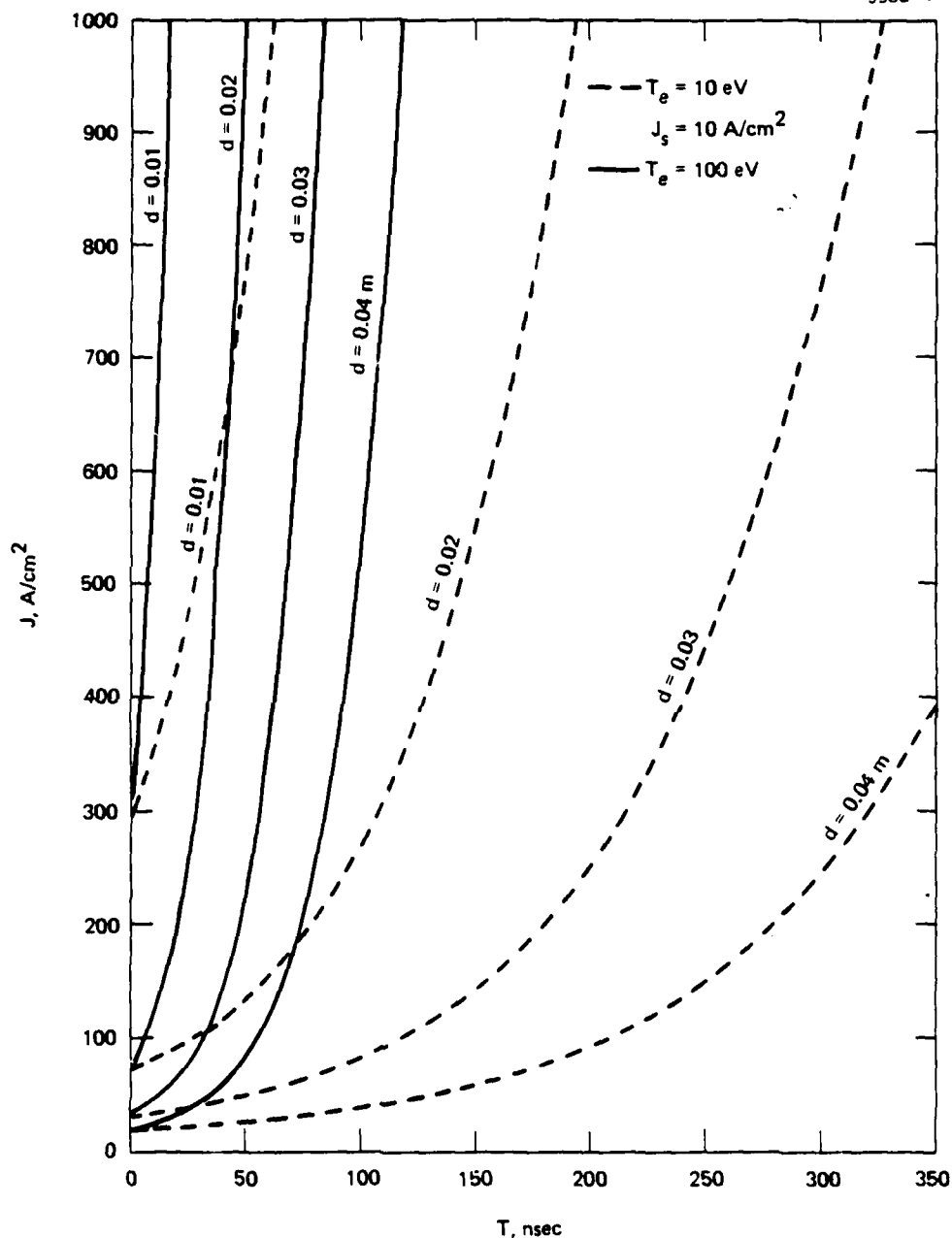
56

9988-1

Figure 24. Anode current density versus time. Initial source current density 10 A/cm^2, at T_e = 10 eV (dashed line) and T_e = 100 eV (solid line.)
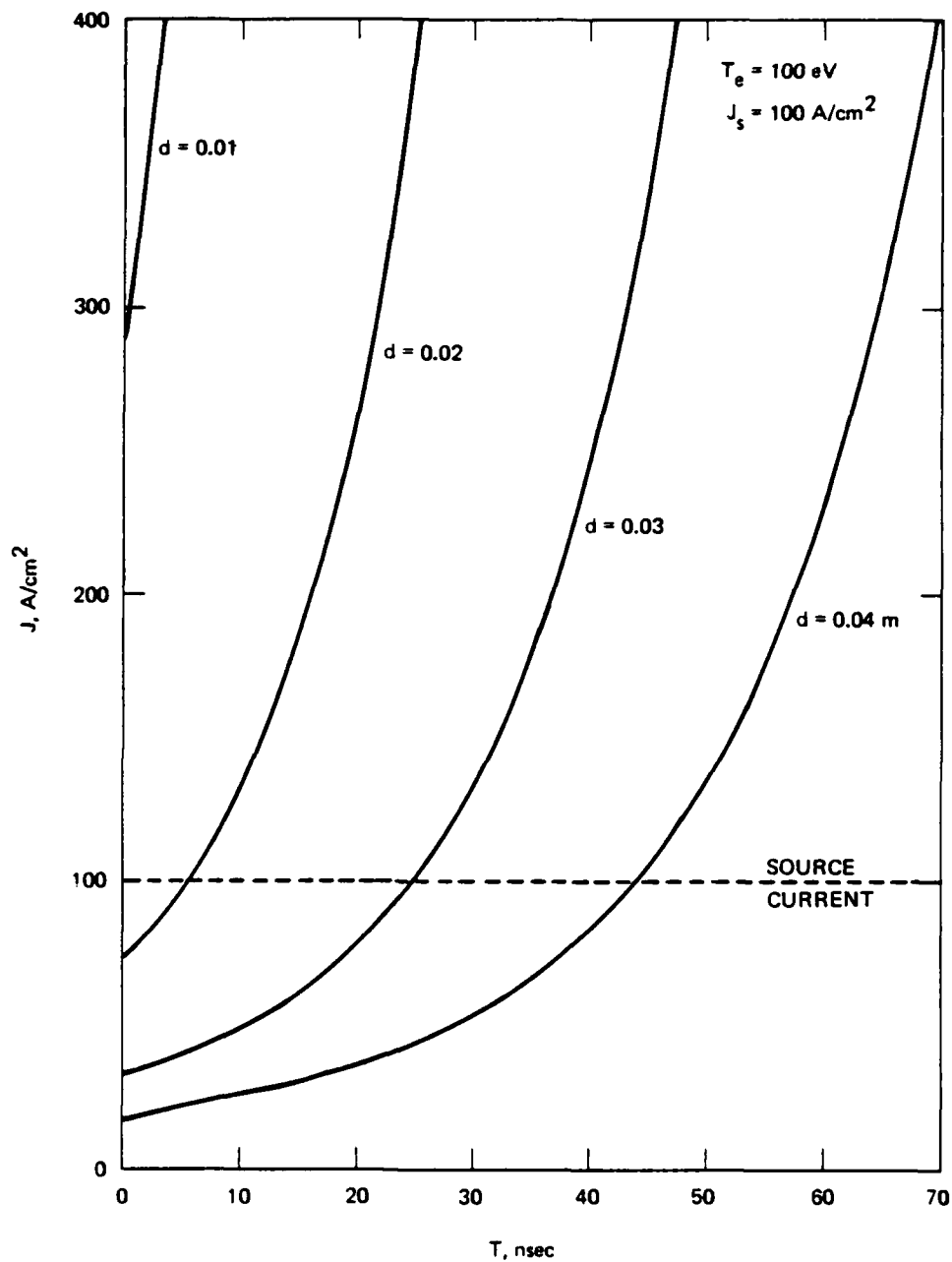
57

Figure 25.   Anode current density versus time.   Initial source
current density 100 A/cm^2 at T_e = 100 eV.
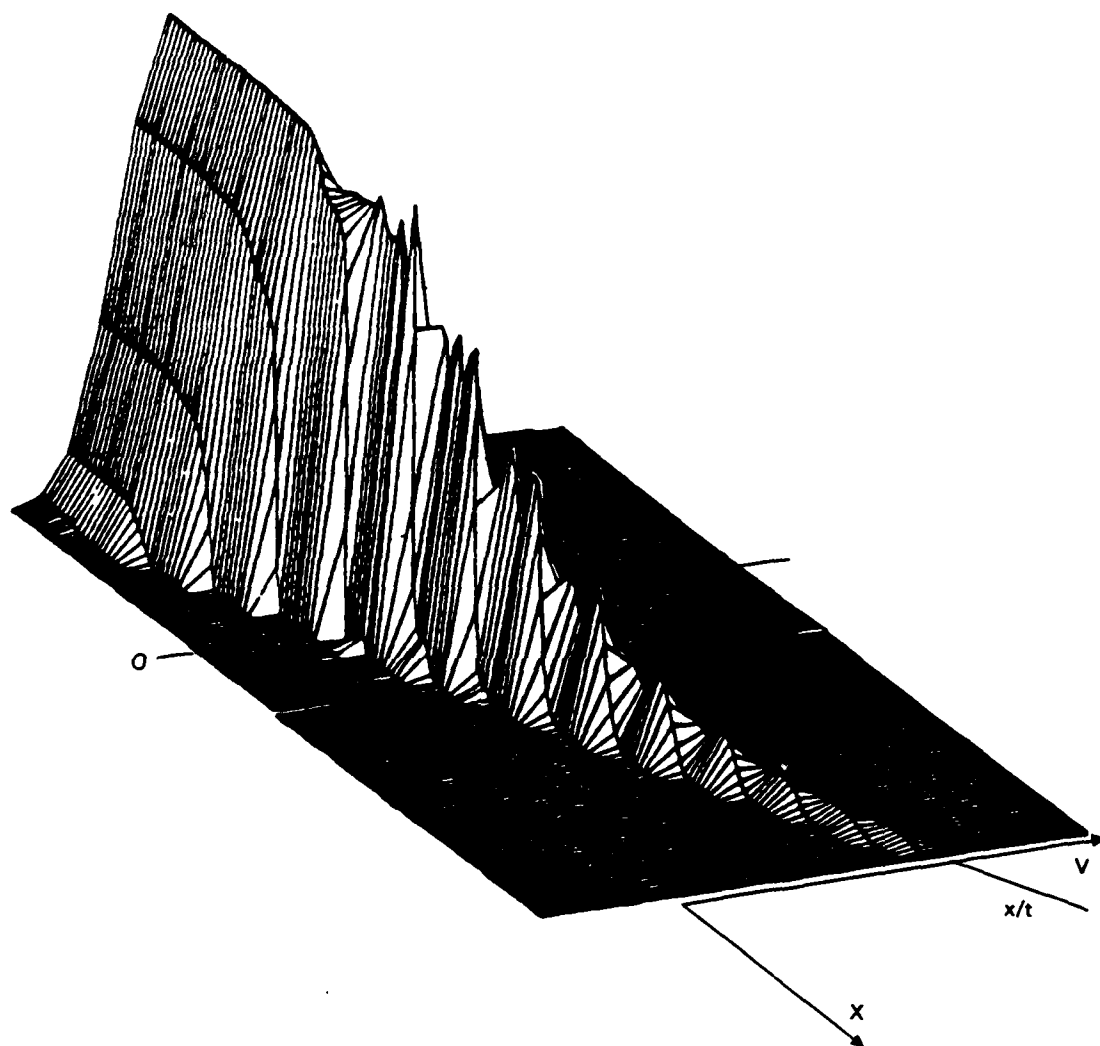
58

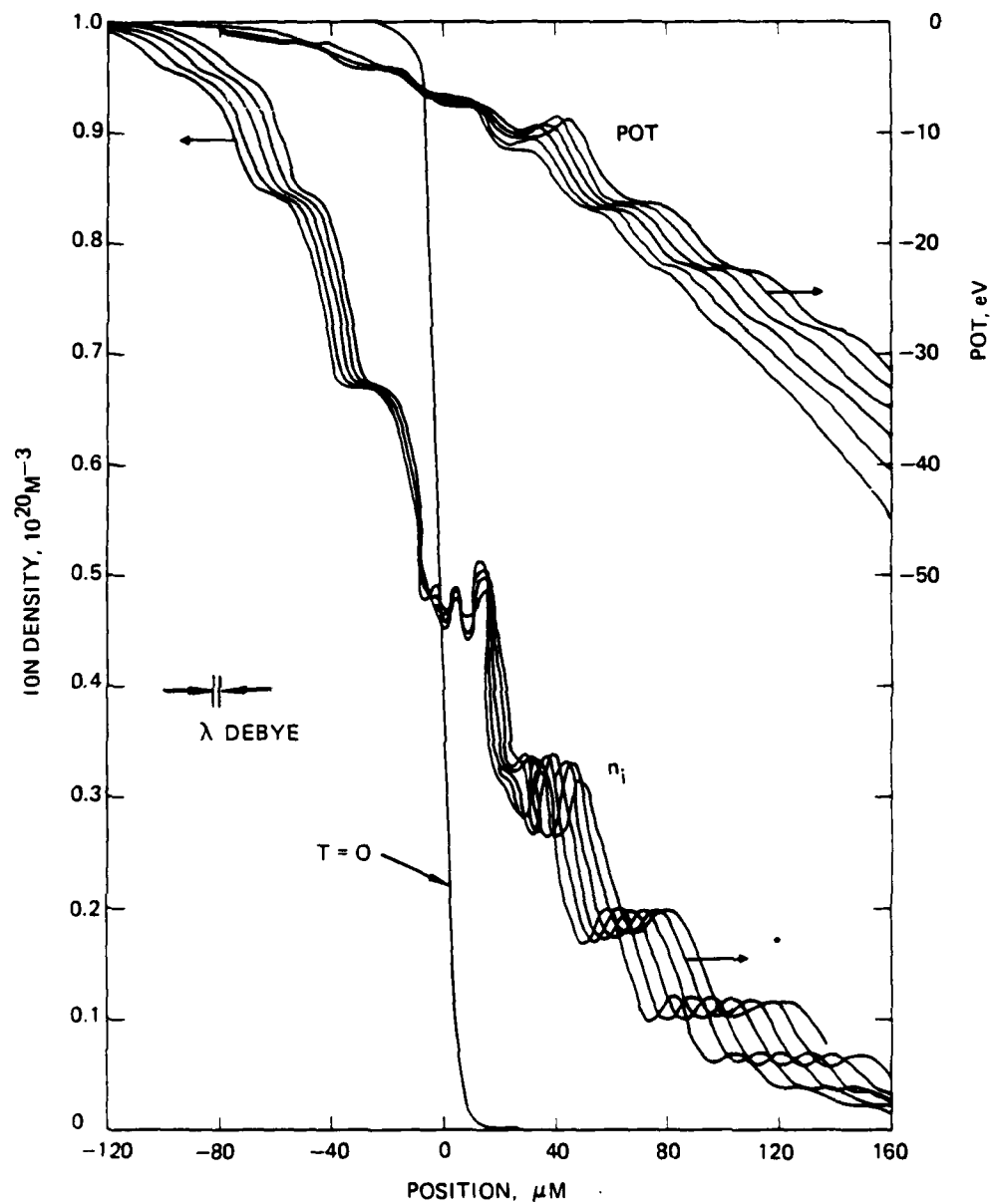Figure 26.   Ion phase space density at 4 nsec.

Figure 27. Progression of ion density and potential with time steps
           of 0.2 nsec. The arrows show the direction of propagation.

60

size in velocity space. The very high frequencies of the center of the
plot are due to a course scale change at 1.8 ns and are the code equiva-
lent of a step function representation. The individual large bumps main-
tain their integrity with time and propagate at well defined velocities
which are skewed in a continuous fashion from the discrete grid veloci-
ties. Thus once formed, they are stable and independent of the grid.
The relationships between the amplitudes of the jumps in the ion density
and in the potential match very well the classical velocity jump condi-
tions across a fluid discontinuity. (The self consistent electronic
space charge supplies the needed compressibility.)

Figure 28 shows the solutions after 4 ns of computation. The
smooth curves are analytical solutions of Eqn. 14 ($x < x_m$) which also
match Eqn. 16 for large x, i.e.,

$$n_i = \frac{n_o \left(1 + (1 + \beta\lambda o)\, d^{\beta x}\right)}{(1 + e^{\beta x})^2} \to n_o\, e^{\beta x} \tag{27}$$

$\beta = 1/v_o t$

$$\frac{m\phi}{kT} = \ln \frac{1}{1 + e^{\beta x}} \to -\beta x \tag{28}$$

The deviation of the calculated solution from the analytical solu-
tion at about $x = 320$ μm is due to the fact that the ions have not had
sufficient time to reach that position. Consequently, the E field is
somewhat enhanced in that region. During the time of calculation the
minimum position accelerated quadratically from rest at first, then it
settled down at a slower linear rise with time ($\sim v_o$) which is well
below the velocity of the approaching ion front ($6.2\ v_o$).

The interesting dynamics of the ions overtaking and distorting the
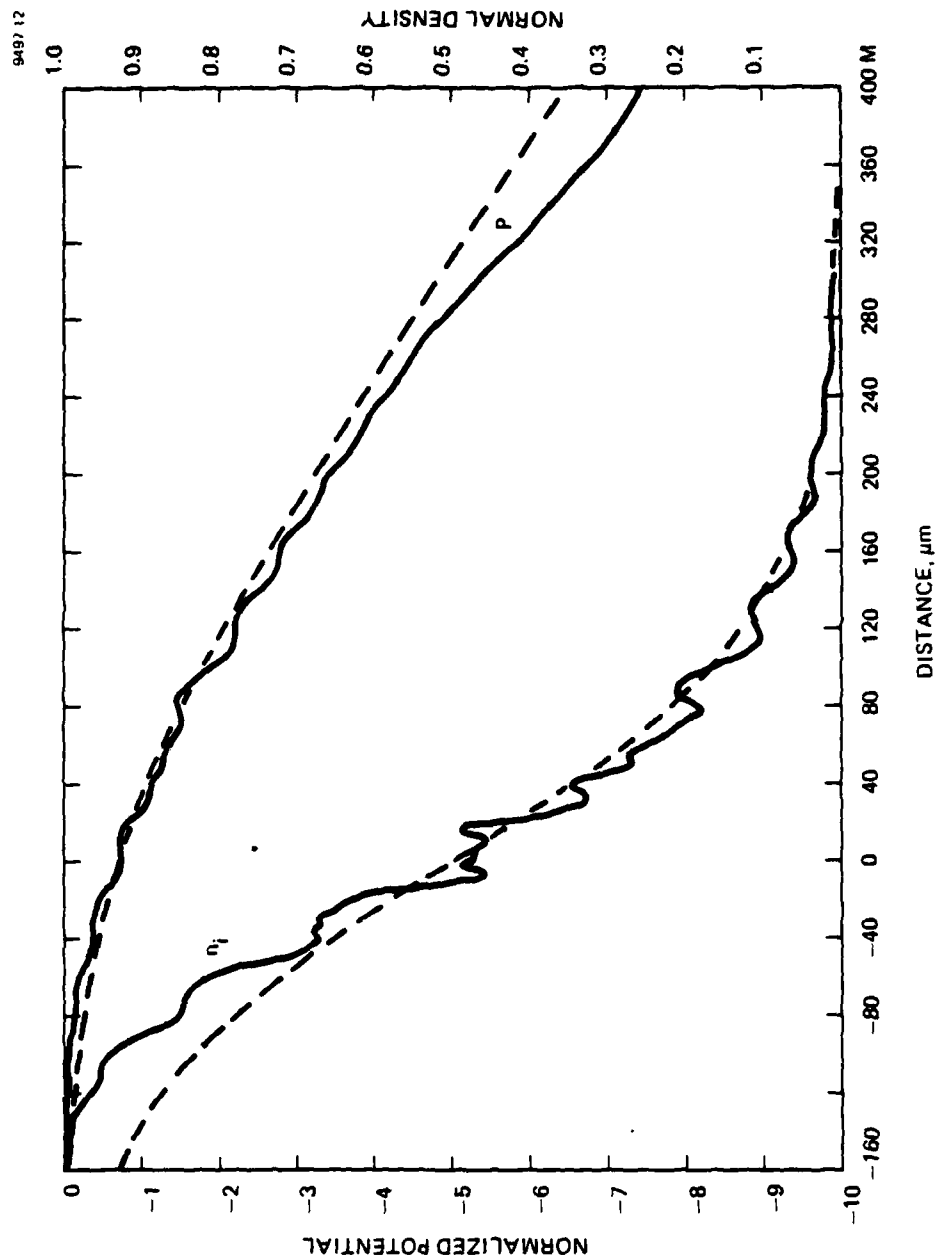minimum potential remains to be simulated. Now that analytical models

Figure 28.   Normalized ion density (n_i/n_o) and normalized potential $(e\phi/kTe)$ after 4 ns of computation (solid curves). Dashed curves are analytical results of equations 27 and 28.

62

are available for the falling portion of the potential, the ever growing burden on the computer storage requirements as the plasma spreads may now be reduced significicnatly.

4. <u>Summary</u>

The theoretical study of the propagation of a plasma released across a vacuum gap into a high electric field shows that closure times of ions $\sim$10 nsec may be anticipated if the effective electron temperature in the source plasma is kept high or a high energy tail is present in the electron velocity distribution. This is consistent with a low operating pressure and a high source current density.[22] The originally anticipated quadratic acceleration of the ion front was not found because the electric field in the front decreases with time as the front spreads. But collective acceleration mechanisms were found which do appear to yield a small (but sufficient number of ions with energies well in excess of the electron thermal energy) to allow a large electron current to cross the gap to the anode in a short time.

63

REFERENCES

1. Private communication with Dr. Richard Briggs (LLL).

2. T.R. Burkes, et al, "A Critical Analysis and Assessment of High Power Switches", September 1978, NP30/78 Final Report to Naval Surface Weapons Center, Dahlgren, UA, Contract No. F33615-77-C-2059.

3. T.R. Burkes, et al, "A Review of High-power Switch Technology", IEEE Trans. Electron Devices, Vol. ED-26, pgs 1401-1410, October 1979.

4. J.E. Thompson, et al, "Investigation of Fast Insulator Surface Flashover", 2nd IEEE International Pulsed Power Conference, Lubbock, TX, 1979, pg 106-113.

5. K.C. Schmidt and C.F. Hendee, "Continuous Channel Electron Multiplier Operated in the Pulse Saturated Mode", IEEE Trans. on Nuclear Science, NS-13, No. 3, pp 100-11, 1966.

6. C.H. De Tourreil and K.D. Srivastava, "Mechanism of Surface Charging of High-Voltage Insulators in Vacuum", IEEE Trans. on Elec. Insulation Vol EI-8, No. 1, March 1973, p. 17-21.

7. A. Faltens, et al, "High Repetition Rate Burst-mode Spark Gap", IEEE Trans Electron Devices, Vol ED-26, pgs 1411-1413, October 1979.

8. J. Kopainsky, "Influence of the Arc on Breakdown Phenomena in Circuit Breakers", pg. 329 in Current Interruption in High Voltage Network, Klaus Ragaller (Ed.) Plenum Press N.Y.

9. J.F. Perkins, IEEE PES Summer Meeting & EHV/UHV Conf., Vancouver, Canada, July 15-20, 1973, paper T73 339-9.

10. J.F. Perkins and L S. Frost, IEEE PES Summer Meeting, San Francisco, CA, July 9-14, 1973, papers: T72 529-6 and C72 530-4.

11. G.A. Farrall and J.D. Cobine, paper 59-334 AIEE Winter Meeting, New York 2/3/59.

12. Earl W. McDaniel & Edward A. Manson, The Mobility and Diffusion of Ions in Gases, pg. 7.

13. Private communication with Dr. F. Rose (NSWC W/O).

14. D.B. Hopkins, "Design Considerations and Data for Gas-Insulated HV Structures", IEEE Pub. No. 75CH1097-5-NPS, 1976 (6th Symp. Eng. Prob. Fusion Res.).

15. Sommerfeld, Mechanics of Deformable Bodies, Academic Press; N.Y. 1950.

16. Landau and Lipshitz, Fluid Mechanics, Addison Wesley, Reading, 1959.

17. Sig Hansen HRL Report #514, Aerodynamics of Gas Blast in the In-Line Circuit Breaker.

18. J.B. Hasted, Physics of Atomic Collisions, American, Elsevier, New York, 1972, pg 615.

19. M. Abramowitz and I.A. Stegun, Handbook of Math Functions, NBS 1964, pg. 298.

20. Courtesy Dr. W. Knauer (HRL).

21. R.K. Parker, R.E. Anderson, and C.V. Duncan, "Plasma Induced Field Emission and the Characteristics of High-Current Relativistic Electron Flow," J.A.P. 45, No. 6, June 1974.

22. S.D. Vagner and B.V. Shlyaev, "Electron Energy Distribution in a Crossed-Field Glow Discharge," Sov. Phys. Tech. Phys. 23(4), 398, April 1978.